

FR-PHENO-2015-004

ELECTROWEAK GAUGE-BOSON PRODUCTION IN ASSOCIATION WITH B JETS AT HADRON COLLIDERS

F. FEBRES CORDERO

*Albert-Ludwigs-Universität Freiburg, Physikalisches Institut
D-79104 Freiburg, Germany
ffebres@physik.uni-freiburg.de*

L. REINA

*Department of Physics, Florida State University,
Tallahassee, Florida, 32306-4350 USA
reina@hep.fsu.edu*

Received (Day Month Year)

Revised (Day Month Year)

The production of both charged and neutral electroweak gauge bosons in association with b jets has attracted a lot of experimental and theoretical attention in recent years because of its central role in the physics programs of both the Fermilab Tevatron and the CERN Large Hadron Collider. The improved level of accuracy achieved both in the theoretical predictions and experimental measurements of these processes can promote crucial developments in modeling b -quark jets and b -quark parton distribution functions, and can provide a more accurate description of some of the most important backgrounds to the measurement of Higgs-boson couplings and several new physics searches. In this paper we review the status of theoretical predictions for cross sections and kinematic distributions of processes in which an electroweak gauge boson is produced in association with up to two b jets in hadronic collisions, namely $p\bar{p}, pp \rightarrow V + 1b$ jet and $p\bar{p}, pp \rightarrow V + 2b$ jets with $V = W^\pm, Z/\gamma^*, \gamma$. Available experimental measurements at both the Fermilab Tevatron and the CERN Large Hadron Collider are also reviewed and their comparison with theoretical predictions is discussed.

Keywords: Quantum chromodynamics; electroweak gauge bosons; bottom quarks; proton-proton inclusive interactions

PACS Nos.: 13.85.Ni, 12.38.Bx, 14.65.Fy, 14.80.Bn

1. Introduction

The production of both charged (W^\pm) and neutral ($Z/\gamma^*, \gamma$) electroweak gauge bosons in association with b jets (generically denoted as $V + b$ -jet production) has attracted a lot of experimental and theoretical attention in recent years because of its central role in the physics programs of both the Tevatron and the Large Hadron Collider (LHC). Many formal developments have improved the accuracy

of theoretical predictions to the level of accuracy necessary to compare with the results that have meanwhile been presented by both the Tevatron and the LHC experiments. In this paper we present an updated review of this topic and collect the most important results that can serve as reference for future studies.

From a physics standpoint W and Z production with b jets is first of all one of the main irreducible backgrounds to the measurement of a Higgs boson in the WH and ZH associated-production channels, which played a leading role for Higgs-boson searches at the Tevatron and will be instrumental in constraining the couplings of the discovered Higgs boson^{1,2} at the LHC. $W + b$ jets is also an important irreducible background in the measurement of single-top production, and $Z + b$ jets can mimic the $H \rightarrow ZZ^* \rightarrow 4l$ (l =lepton) final state when associated B mesons decay leptonically. In general, electroweak vector bosons (namely W^\pm and Z) and b quarks often appear in the decay chain of heavy massive particles in models beyond the Standard Model (SM), making of the $V + b$ -jet processes important backgrounds for searches of new physics at the LHC.

At the same time, the production of a SM vector boson (W^\pm , Z/γ^* , and γ) with heavy quarks (both b and c) is per se an important test of QCD for two main reasons. The first reason is that it allows to study the dynamics of b (and c) jets and improve their modeling in many other more challenging SM processes that represent important backgrounds to new physics searches (consider for example $t\bar{t} + b$ jets). The second important reason is that the production of W^\pm , Z/γ^* , and γ with heavy quarks (b and c) offers a unique possibility to measure the bottom- and charm-quark parton distribution functions (PDF) using only collider data, as will become clearer (for the b case) from a closer inspection of the parton-level processes that are at the core of $V + b$ -jet production.

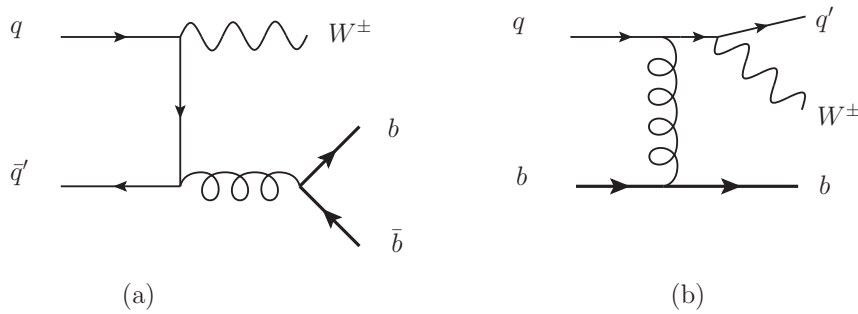


Fig. 1. Examples of tree-level Feynman diagrams contributing to $W^\pm + b$ signatures at hadron colliders, without and with contributions from initial-state b quarks.

The parton-level structure of $V + b$ jets differs for charged ($V = W^\pm$) and neutral ($V = Z/\gamma^*, \gamma$) gauge bosons. Furthermore, such structure depends on the number

of light flavors ($N_f = 4$ or $N_f = 5$) that are allowed in the initial-state hadrons (p and \bar{p}). Given the non-negligible mass of the bottom quark ($m_b \gg \Lambda_{QCD}$), the question of considering a massless bottom quark with an initial-state parton density in the (anti)proton is non trivial and is intuitively related to the energy scale of the process considered. Since typically $V + b$ -jet processes involve a range of energies from few tens to few hundreds of GeV, the answer is not clear cut and the problem cannot be addressed without considering the perturbative QCD structure of the corresponding physical observables (total and differential cross sections), as we will discuss in more detail in Section 2. Considering only the first-order (or tree-level) processes, let us remind the reader that $W^\pm + 2b$ jets can proceed only through $q\bar{q}' \rightarrow W^\pm b\bar{b}$ (see Figure 1.a), while $W^\pm + 1b$ jet can proceed through the same channel if we assume $N_f = 4$ and also through $bq \rightarrow W^\pm b + q'$ (see Figure 1.b) if we assume $N_f = 5$. Similarly, $Z/\gamma + 2b$ jets can only proceed (at lowest order in α_s) through $q\bar{q} \rightarrow Z/\gamma b\bar{b}$ and $gg \rightarrow Z/\gamma b\bar{b}$ (see Figure 2.a), while $Z/\gamma + 1b$ jet can proceed through the same processes if we assume $N_f = 4$, or through $bg \rightarrow bZ/\gamma$ if we assume $N_f = 5$ (see Figure 2.b). Notice that in this discussion we keep only the Cabibbo sector of the flavor-mixing CKM matrix and neglect processes initiated by two b (anti)quarks (like e.g. $b\bar{b} \rightarrow \gamma b\bar{b}$). These approximations have effects at the 1% level in the observables studied. The diagrams in Figures 1.b and 2.b clearly illustrate the possibility of measuring the b -quark PDF by measuring $V + b$ -jet processes.

On the theoretical side, total and differential hadronic cross sections including Next-to-Leading Order (NLO) QCD corrections have been first calculated for $W^\pm b\bar{b}$ and $Zb\bar{b}$ production in the limit of zero bottom-quark mass,^{3,4} followed more recently by fully massive calculations ($m_b \neq 0$) for $W^\pm b\bar{b}$,⁵⁻⁷ $Zb\bar{b}$,^{6,8} and $\gamma b\bar{b}$ ⁹ production. The NLO QCD calculations of $W^\pm b\bar{b}$ hadronic production (for $m_b \neq 0$), including spin-correlation effects from $W \rightarrow l\nu_l$ decay,⁷ and of $Z/\gamma^* b\bar{b}$ (with $m_b = 0$ and $Z/\gamma^* \rightarrow l^+l^-$) are available in MCFM.¹⁰ These NLO QCD corrections can now also be calculated with several automated tools like for example `MadGraph5_aMC@NLO`,¹¹ and `SHERPA`¹² in conjunction with `GoSam`¹³ or `OpenLoops`.¹⁴ A study of $W^\pm b\bar{b}$, and $Z/\gamma^* b\bar{b}$ production at hadron colliders, including NLO QCD corrections, m_b effects, and spin-correlation effects from W and Z decays, as well as the interface with parton-shower Monte Carlo generators like `PYTHIA`^{15,16} and `HERWIG`^{17,18} via the `MC@NLO` method,^{19,20} has been presented in Ref. 21. The NLO QCD calculation of $pp, p\bar{p} \rightarrow W^\pm b\bar{b}$ from Refs. 5 and 6 has also been interfaced with `Pythia` and `Herwig` using the `POWHEG` method,^{22,23} and is available in the `POWHEG BOX` framework.²⁴ Recently the NLO QCD hadronic cross section for $W^\pm b\bar{b} + j$ has been implemented in the `POWHEG BOX`²⁵ (see also the calculation of the corresponding $O(\alpha_s)$ virtual corrections presented in Ref. 26).

Higher-order QCD corrections are also known for the $N_f = 5$ processes. In particular the first complete calculation of W^\pm hadronic production with at least one b jet ($pp, p\bar{p} \rightarrow W + b + X$), including NLO QCD corrections and full b -mass effects,

4 Febres Cordero, and Reina

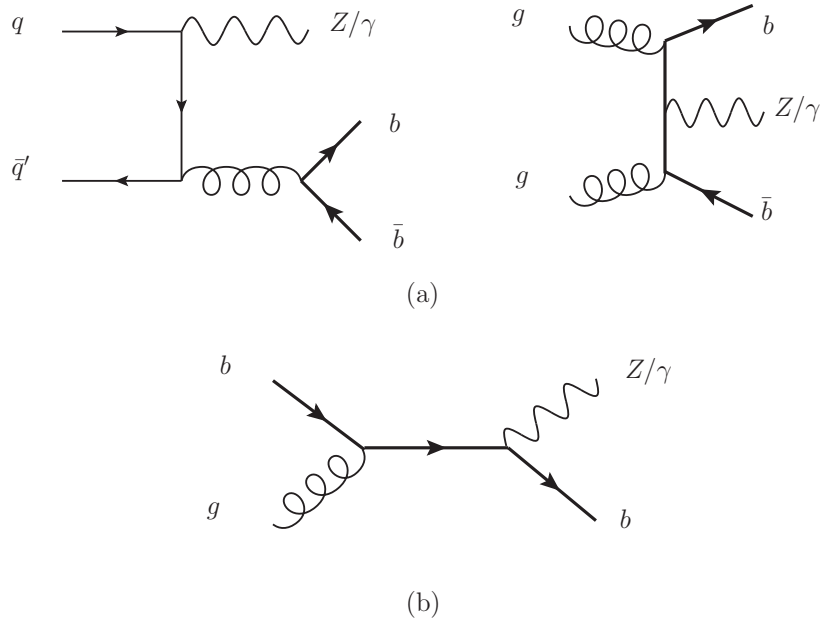


Fig. 2. Examples of tree-level Feynman diagrams contributing to $Z/\gamma b$ signatures at hadron colliders, without and with contributions from initial-state b quarks.

has been presented in Ref. 27, updated in Ref. 28, and is now available through MCFM.¹⁰ The calculation was based on separate contributions from Refs. 29, 5, 6, and 7. NLO QCD corrections to Z hadronic production with one b jet ($pp, p\bar{p} \rightarrow Z + b$) and with at least one b jet ($pp, p\bar{p} \rightarrow Z + b + X$) have been calculated in Refs. 30 and 31 respectively, and are available through MCFM. Finally, the hadronic production of a photon and one b jet ($pp, p\bar{p} \rightarrow \gamma + b$) at NLO QCD has been calculated in Ref. 32 and independently cross-checked in Ref. 9. Some of these processes are now being computed using automated NLO QCD parton-shower Monte Carlos like e.g. `MadGraph5_aMC@NLO`,^a although some aspects of the parton-shower generation in the $N_f = 5$ scheme still need to be studied, as we will discuss in Section 2.

On the experimental side, both the CDF and D0 experiments at the Tevatron as well as the ATLAS and CMS experiments at the LHC have provided a variety of results for $V + 1b$ -jet and $V + 2b$ -jet production, both with and without extra light jets. At the Tevatron, the cross section for $W^\pm + 1b$ jet has been measured by both CDF³³ and D0.^{34,35} CDF has also measured the cross section for $Z + 1b$ jet,³⁶ and D0 the ratio of the cross sections for $Z + b$ jets and $Z + j$ (j =light jets). The production of³⁷ $\gamma + 1b$ jet has further been measured by CDF³⁸ and D0,^{39,40} as

^a Results from `MadGraph5_aMC@NLO` have been published in ATLAS and CMS papers as we will summarize in Section 3

well as of $\gamma + 2b$ jets by D0.⁴⁰ At the LHC, we now have measurements of $W^\pm + 1b$ jet and $W^\pm + 2b$ jets from ATLAS,^{41,42} and of $W^\pm + 2b$ jets from CMS,⁴³ as well as of $Z + 1b$ jet and $Z + 2b$ jets from both ATLAS^{44,45} and CMS.^{46–48} We will summarize the most relevant aspects of these experimental studies including the exact definition of the signal signatures in Section 3.

The rest of the paper is organized as follows. We briefly review in Section 2 the main structure of the $V + b$ -jet cross sections, including the first order of QCD corrections, for both $N_f = 4$ and $N_f = 5$. In Section 2 we also discuss the uncertainties associated with the theoretical predictions for these processes, and present more specific theoretical issues, like photon isolation, which is relevant for $\gamma + b$ -jet production. A selection of the most recent experimental results will be presented in Section 3 with particular emphasis on the comparison between theory and experiments as presented in each of the selected measurements. Section 4 contains our conclusions and outlook.

2. Theoretical Framework

In this Section we review the most important aspects of the calculation of the hadronic cross section for $V + 1b$ jet and $V + 2b$ jet production ($V = W^\pm, Z/\gamma^*, \gamma$) at NLO in QCD. In particular we focus on the meaning of presenting results in the four- ($N_f = 4$, denoted as 4F) and five-flavor ($N_f = 5$, denoted as 5F) schemes, on the matching of the corresponding parton-level calculations with existing parton-shower Monte Carlo generators, and on the assessment of the theoretical uncertainties associated with different stages of the calculation. We will substantiate our discussion with results taken from various theoretical studies presented in the literature, and refer to the corresponding sources for further details. Several important aspects of existing theoretical studies are illustrated using the experimental results collected in Section 3.

2.1. Four- and five-flavor schemes

Four- and five-flavor schemes differ by the number of partons that are allowed to have a non-zero parton distribution function in the colliding hadrons. Since the bottom quark ($m_b \gg \Lambda_{QCD}$) lives in the perturbative regime of QCD, the issue of defining a bottom-quark parton density is non trivial, and is intuitively related to the energy scale of the process considered. It is important to understand the relation between the two schemes and emphasize that they are just different prescriptions to calculate the same physical processes ($V + b$ -jet hadronic production in our case) in perturbative QCD. One can indeed tailor the arrangement of the perturbative expansion of the cross sections to specific energy regimes, where some classes of corrections may become more important than others. Since 4F and 5F correspond to different rearrangements of the perturbative expansion of the cross section for a given process, the two prescriptions share more terms the higher the perturbative order, and in some cases significant differences can still appear at NLO in QCD. A

recent systematic study of 4F versus 5F schemes has been presented in Ref. 49, to which we refer for more details.

$V + b$ -jet hadronic processes offer indeed a broad range of examples and very effectively lend themselves to illustrate the range of validity of fixed-order calculations using either the 4F or the 5F approaches. Given the multi-scale nature of $V + b$ -jet processes, the accurate theoretical description of these processes requires to consider the perturbative QCD structure of the corresponding physical observables (total and differential cross sections) in detail. We will return to this point with specific examples after having defined more in detail how 4F and 5F schemes are implemented in the actual calculation of $V + b$ -jet hadronic production.

In the 4F scheme, the initial-state quarks are constrained to be the four lightest quarks (taken to be massless), there are no bottom quarks in the initial state, and the final-state bottom quarks are considered massive. Both $V + 2b$ -jet and $V + 1b$ -jet processes receive contributions at lowest order in QCD from $q\bar{q}$ and gg initiated subprocesses, specifically from $q\bar{q}' \rightarrow W^\pm b\bar{b}$ in the case of W^\pm , and $q\bar{q} \rightarrow Z/\gamma b\bar{b}$ and $gg \rightarrow Z/\gamma b\bar{b}$ in the case of Z and γ . Cross sections are computed at fixed order in QCD (LO, NLO, etc.) and the number of b jets in the final state is selected applying specific kinematic cuts on the transverse momentum ($p_T^{b\text{jet}} > p_T^{\text{min}}$) and, possibly, the rapidity/pseudorapidity ($|y^{b\text{jet}}| < y^{\text{max}}$ or $|\eta^{b\text{jet}}| < \eta^{\text{max}}$) of the final-state b jets, where it is understood that a given jet algorithm is in place to select the final-state b jets and light jets.^b At NLO in QCD the cross section for $Vb\bar{b}$ production receives contributions from both the lowest order processes listed above and the corresponding $O(\alpha_s)$ virtual and real corrections, more specifically:

- one-loop *virtual* corrections to $q\bar{q}' \rightarrow W^\pm b\bar{b}$ and $q\bar{q}, gg \rightarrow Z/\gamma b\bar{b}$, respectively;
- one additional parton *real* emission processes, i.e. $q\bar{q}' \rightarrow W^\pm b\bar{b} + g$ and $q\bar{q} \rightarrow W^\pm b\bar{b} + q'$ in the case of $W^\pm b\bar{b}$ production; as well as $q\bar{q}, gg \rightarrow Z/\gamma b\bar{b} + g$ and $q\bar{q} \rightarrow Z/\gamma b\bar{b} + q$ in the case of $Z/\gamma b\bar{b}$ production (notice that for convenience we denote by qg also the corresponding $\bar{q}g$ channels).

In the 5F scheme, the definition of a bottom-quark PDF arises because the integration over the phase space of non-identified final-state bottom quarks (as in the case of $V + 1b$ -jet processes) gives origin to potentially large logarithms of the form:

$$\Lambda_b \equiv \ln \left(\frac{\mu^2}{m_b^2} \right) , \quad (1)$$

where μ is a scale related to the upper bound on the integration over the transverse momentum, p_T , of the final-state bottom quark,^c while the dependence on m_b comes from the limit of producing a b quark with no transverse momentum. This happens

^bWe notice that in a parton-level calculation, even at NLO in QCD, these jets have very limited structure.

^cThe symbol μ is often used to suggest the possibility of setting this upper bound to be the factorization scale of the bottom-quark PDF to be defined in the next paragraph.

when a final-state bottom-quark pair is produced via $g \rightarrow b\bar{b}$ splitting of an initial-state gluon, and corresponds to the collinear singularity that would be present in the case of a gluon splitting into massless quarks ($m_b \rightarrow 0$). For scales μ of $\mathcal{O}(M_V)$ or larger these logarithms can be quite large. Additionally, the same logarithms appear at every order in the perturbative expansion of the cross section in the strong coupling, α_s , due to recursive gluon emission from internal bottom-quark lines, as well as virtual corrections. These logarithms could hinder the convergence of the perturbative expansion of the total and differential cross sections. In the 5F the convergence is improved by introducing a perturbatively-defined bottom-quark PDF,^{50–52} defined at lowest order in α_s as,

$$\tilde{b}(x, \mu) = \frac{\alpha_s(\mu)}{2\pi} \Lambda_b \int_x^1 \frac{dy}{y} P_{qg} \left(\frac{x}{y} \right) g(y, \mu) , \quad (2)$$

where $g(y, \mu)$ is the gluon PDF and P_{qg} is the Altarelli-Parisi splitting function for $g \rightarrow q\bar{q}$ given by,

$$P_{qg} = \frac{1}{2} [z^2 + (1-z)^2] . \quad (3)$$

The Λ_b logarithms are subsequently resummed through the DGLAP evolution equation,^{53–55} such that contributions proportional to $(\alpha_s \Lambda_b)^n$ can be absorbed, to all orders in n , into a leading-logarithm bottom-quark PDF, while subleading logarithms are recursively resummed when higher-order corrections are considered in the DGLAP equation. With the use of a bottom-quark PDF, the 5F effectively reorders the perturbative expansion to be one in α_s and Λ_b , or $\alpha_s \Lambda_b$. In those kinematic regimes where $\alpha_s \Lambda_b$ is not a small expansion parameter, the use of a bottom-quark PDF should improve the stability of the total and differential cross sections. As observed in Ref. 49, however, the argument of the Λ_b logarithms, as it arises from the collinear limit of $g \rightarrow b\bar{b}$ in 4F processes, is often not a constant, but contains some dependence on the momentum fraction carried by the gluon (y in Eq. 2), which can considerably reduce the relevance of such logarithmic terms at each perturbative order. General arguments to estimate their relevance at all perturbative orders are given for $2 \rightarrow 1$ and $2 \rightarrow 2$ processes in Ref. 49.

In the 5F, while the production of $V + 2b$ jets mainly receives contributions from light-quark- and gluon-initiated processes (processes like $b\bar{b} \rightarrow Zb\bar{b}$ are negligible), the case of $W^\pm + 1b$ jet and $Z/\gamma + 1b$ jet have rather different characteristics. $Z/\gamma + 1b$ jet starts at LO with $bg \rightarrow Z/\gamma b$, where, according to our previous discussion, the initial state b -quark density has been introduced to resum the large logarithms arising in the calculation of $gg \rightarrow Z/\gamma b\bar{b}$, when one of the b quarks in the $g \rightarrow b\bar{b}$ splitting gives origin to a b jet that is not tagged. At lowest order it corresponds to \tilde{b} in Eq. (2). At NLO the following $O(\alpha_s)$ corrections are then to be added:

- one-loop *virtual* corrections to $bg \rightarrow Z/\gamma b$ (notice that for convenience when we write $b(q)$ in the initial state we mean generically processes initiated by both $b(q)$ and $\bar{b}(\bar{q})$);

8 *Febres Cordero, and Reina*

- one additional parton *real* emission processes: $bg \rightarrow Z/\gamma b + g$, $bq \rightarrow Z/\gamma b + q$, $q\bar{q} \rightarrow Z/\gamma b\bar{b}$, and $gg \rightarrow Z/\gamma b\bar{b}$.

On the other hand, in $W^\pm + 1b$ -jet production the first b -initiated subprocess starts as a $2 \rightarrow 3$ process ($bq \rightarrow W^\pm bq'$) because the first gluon-initiated subprocess is higher order ($qg \rightarrow W^\pm b\bar{b} + q'$). Therefore, there are two competing LO subprocess, namely $q\bar{q}' \rightarrow W^\pm b\bar{b}$ and $bq \rightarrow W^\pm bq'$ and the NLO QCD cross section includes the following $O(\alpha_s)$ corrections:

- one-loop *virtual* corrections to $q\bar{q}' \rightarrow W^\pm b\bar{b}$;
- one-loop *virtual* corrections to $bq \rightarrow W^\pm bq'$;
- one additional parton *real* emission processes: $q\bar{q}' \rightarrow W^\pm b\bar{b} + g$, $qg \rightarrow W^\pm b\bar{b} + q'$, $bq \rightarrow W^\pm bq' + g$, and $bg \rightarrow W^\pm bqq'$.

One can notice that the subprocesses and corrections contributing to the 4F NLO cross section for $W^\pm + 1b$ -jet production are a subset of those contributing to the 5F NLO cross section, while this is not true for $Z/\gamma + 1b$ jet. In the case of $W^\pm + 1b$ we can then state that the most complete NLO QCD prediction is the 5F one, while in the case of $Z/\gamma + 1b$ jet it very much depends on the relevance of the logarithms that are resummed in the 5F approach as compared to the non-logarithmic terms that are neglected in the 5F but not in the 4F.

We also notice that special attention needs to be paid in combining tree-level and higher-order corrections in order to avoid double counting of Λ_b logarithms that appear both in a fixed-order process (like, e.g. $gg \rightarrow Zb\bar{b}$) from gluon splitting, and in the corresponding b -initiated subprocess (like, e.g. $bg \rightarrow Zb$) from the expansion of the b -quark PDF. Double counting is avoided by introducing a *subtraction term* that removes from the the fixed-order cross section of a b -initiated process the logarithmic term(s) already resummed in the b -quark PDF. For example, the NLO QCD cross section for $Z + 1b$ jet in the 5F should be calculated as,

$$\sigma_{5F}^{\text{NLO}}(Z + 1b) = \sigma_{bg}^{\text{LO}} + \sigma_{bq}^{\text{NLO}} - \int dx_1 dx_2 \tilde{b}(x_1, \mu) g(x_2, \mu) \sigma_{bq}^{\text{LO}}, \quad (4)$$

where the last term is the NLO subtraction term which avoids double counting of the Λ_b logarithm already included in the lowest order b PDF given in Eq. (2).

It is clear by looking at the different perturbative structure of the calculation of $W^\pm b\bar{b}$ vs. $Z/\gamma b\bar{b}$ production that we can expect 4F or 5F predictions to give a more accurate prediction of these processes depending on the energy (Tevatron vs. LHC) and kinematical regime. Apart from more specific situations on which we will comment in Section 3 when we discuss the comparison of existing experimental measurements to the corresponding theoretical predictions, we can conclude this synopsis of 4F vs. 5F by emphasizing some general criteria. First of all, it is worth emphasizing one more time that $V + 2b$ -jet processes are very well described in the 4F at NLO in QCD. This is clear by a simple inspection of the contributing parton-level processes and is supported by the measurements of $W + 2b$ jets (see Table 2 and Figure 3), $Z/\gamma^* + 2b$ jets (see Table 4 and Figures 5 and 6), and $\gamma + 2b$ jets (see

Figure 9). On the other hand, for $V + 1b$ -jet processes 4F and 5F approaches can be complementary. In general, a 5F approach lends itself better to the calculation of more inclusive quantities (like total cross sections) and, in this case, it often allows to push the perturbative fixed order slightly higher since, in most cases, it involves simpler processes. At the same time a 4F approach can be preferable for the calculation of more exclusive observables, like processes with more than a single heavy jet in the final state.

There are however cases in which one approach can be clearly preferable than the other beyond general considerations. For instance, processes that, at a given energy or in a given kinematical regime, are determined at LO by $q\bar{q}$ -initiated subprocesses will be less sensitive to large logarithms Λ_b that have their origin in the integration over the low- p_T region of b quarks produced in $g \rightarrow b\bar{b}$ initial-state splitting. This is for instance the case of $W + b$ jet, where the sensitivity to Λ_b -like logarithms is indeed a NLO effect (see results in Table 2 and Figures 3 and 4), or the case of $\gamma + b$ -jet production at the Tevatron, where the $q\bar{q}$ -channel dominates over the gg -channel production (see results in Figures 7, 8 and 9).

Ideally, a 5F calculation with sufficiently high orders of QCD corrections included would give the best of both worlds, since it would include both enough fixed-order non-logarithmic terms (also present in the corresponding 4F calculation) and the resummation of several orders of potentially large initial-state logarithms. The more perturbative orders are included the broader is the overlap between 4F and 5F predictions for a given cross section. It is in general a good sanity check to assure that the 4F and 5F predictions confirm the existence of such overlap by showing more and more compatibility in going from LO to NLO, or, if needed, to higher order.

2.2. Theoretical uncertainties

Theoretical predictions are affected by both perturbative and non-perturbative uncertainties. On one hand, hard-scattering cross sections are inherently approximate since they are calculated at a given order in perturbative QCD, while the algorithms adopted to implement the following radiation of partons (parton showering) are based on the approximation of accounting only for those phase-space regions that most contribute to extra-parton radiation. On the other hand, all hadronization models adopted to describe the formation of hadronic bound states after the last stages of parton showering contain some level of arbitrariness.

At the parton level, the main sources of theoretical uncertainty are the dependence on the renormalization and factorization scales (μ_R, μ_F) of the NLO QCD cross sections as well as their dependence on the choice of PDF and α_s . The dependence on the choice of m_b can also be sizable and comparable at times to the systematic uncertainty from PDF and α_s . This has been documented for instance in some $W + b$ -jet studies,^{7,28} but is otherwise usually neglected in experimental studies. Looking at the theoretical predictions reported in Tables 2 and 4, we can see

that uncertainties due to scale variation are typically at the 10-25% level, depending on the process, while the uncertainty from PDF and α_s is closer to 2-8%. On the other hand, from the entry in Table 2 we see that D0 estimates the uncertainty due to m_b at the 5% level.

It is difficult to summarize the scale dependence of different $V + b$ -jet processes in a way that could fit the various experimental frameworks in which they are measured, since the behavior of the theoretical predictions depends in part on the specific signatures required by the experiments. There are however some general characteristics that only depend on the intrinsic QCD structure of these processes and we will review them here. In Section 3 we complement this information by collecting in Tables 2 and 4 existing experimental results and the quoted theoretical predictions, including their uncertainties, and we will add comments on the specific of each case if necessary.

From several general studies appeared in the literature over the last few years^{5-9,27,28} we can see that the cross section for all $V + 2 b$ -jet processes shows a large residual scale dependence even after full NLO QCD corrections have been included. As explained in Section 2.1 the calculation of $V + 2 b$ jets is a 4F-only result, and the residual scale dependence is mainly due to the opening of a new qg channel ($qg \rightarrow Vb\bar{b} + q^{(\prime)}$) at NLO. This subprocess contributes to the $O(\alpha_s)$ real corrections of $Vb\bar{b}$ production and, as a tree level process, affects the cross section with the large scale uncertainty of a LO process. This is most visible in the case of $W^\pm b\bar{b}$ production, since at LO $W^\pm b\bar{b}$ is only $q\bar{q}'$ - not gluon-induced. At the LHC, where the gluon density dominates over the light-quark densities, qg -initiated processes are enhanced compared to $q\bar{q}$ processes and the impact of the qg -initiated $O(\alpha_s)$ corrections induce a large scale dependence of the NLO cross section. This effect is milder, although still very visible, for $Z/\gamma + 2 b$ -jet production, since the corresponding LO processes already contain a qg -initiated channel (see Figure 2), and are therefore less affected by the opening at NLO of a qg channel. This has been observed and carefully discussed in Refs. 5, 6, and 8.

On the other hand, NLO theoretical predictions for $V + 1b$ -jet production show in general a more stable behavior with respect to renormalization- and factorization-scale variations when calculated in the 5F, since the logarithmic resummation introduced via the b -quark PDF also resums scale-dependent logarithmic corrections and, as a side effect, improves the scale dependence of the cross section. On the other hand, the 4F predictions of $V + 1b$ -jet production show the same large scale dependence as the corresponding $V + 2b$ -jet results. This was studied in Refs. 27, 28 for $W + 1b$ -jet production and can also be seen for the case of $Z + 1b$ -jet production in Table 4 where results for $Z + 1b$ jet production in both the 5F and 4F schemes are reported.

The second major source of theoretical uncertainty at parton level is the dependence on the PDF with which the parton-level cross section is convoluted to produce the hadronic cross section. In the 4F the systematic uncertainty from PDF is due to

the accuracy of light-quark and gluon parton densities. In the 5F the same is true since the bottom PDF is defined in terms of the gluon and light-quark PDF. In both cases, the uncertainty induced on total and differential cross sections is of the order of 2-8% (see Tables 2 and 4), smaller than the uncertainty from scale dependence, and it will probably further improve in the future. Still, the theoretical uncertainty from PDF and α_s has not been systematically and consistently implemented in all experimental studies. Many results are still compared to theoretical predictions that use specific PDF (without comparing to others), or do not distinguish between differences due to the choice of α_s and of the PDF set.

In particular, the dependence on the b -quark PDF needs to be addressed more carefully. Indeed we need to remember that the $V+b$ -jet processes can play a leading role in *measuring* the b -quark PDF, providing the first such direct determination and therefore testing the range of validity of a purely perturbative definition of the b -quark PDF in terms of gluon and light-quark parton densities. It is therefore crucial to determine the precision with which the b -quark PDF itself can be extracted from $V+b$ -jet measurements. A careful determination will have to consider all available $V+b$ -jet processes and try to select a sample of measurements that provide enough information, when compared with theoretical predictions, to disentangle light-quark, gluon, and b -quark initiated processes. Typically, separating samples with two b jets from samples with one b jet, as well as disentangling single b -jet events in which the b jet contains two almost collinear b quarks or a single b quark can be very helpful. To this extent some theoretical studies^{27,28} have reported predictions for each sample separately, and recent experimental analyses, like Ref. 56, accounts for the study of techniques developed to tag so called merged (bb) jets.

Finally, it is important to mention one last source of parton-level theoretical uncertainty, namely the effects due to double-parton scattering,⁵⁷ that has been only recently formally included in the theoretical prediction for $W^\pm + 2b$ jets and $Z/\gamma^* + 2b$ jets. Double-parton scattering, where a $V + 2b$ ($V = W^\pm, Z/\gamma^*$) parton-level final state is produced as the result of two scattering processes ($q\bar{q}^{(\prime)} \rightarrow V$ and $q\bar{q}, gg \rightarrow b\bar{b}$), can give a substantial contribution when the constituent subprocesses have very large cross sections (as is the case for dijet or $b\bar{b}$ production). The factorization on which this estimate is based, however, is a rather crude approximation and relies on the measurement of the effective-cross-section parameter (σ_{eff}) for hard double-parton interactions. The large uncertainty that still affect such measurement⁵⁸ induces a sizable error on the corresponding $V+b$ -jet cross sections (see e.g. Table 2).

Beyond the parton level, the best theoretical predictions can be obtained via NLO QCD event generators (e.g. MC@NLO, POWHEG, SHERPA) that interface NLO QCD parton-level calculations with parton-shower Monte-Carlo event generators. In this context, care must be taken to assess and quantify the systematic uncertainties introduced by the parton-shower algorithms and by the hadronization and underlying-event models used. This is a non trivial task and need to be addressed on a process by process basis, taking into account the specifics of the generator used

and of the experimental set up. Nevertheless, general tests aimed at estimating the dependence of the theoretical prediction on parameters intrinsic to the showering algorithms (like scale parameters other than renormalization and factorization scales) or the hadronization model should be always performed and the corresponding variations should be understood, confirmed by different approaches (i.e. codes), and included in the theoretical systematics. Several of the results that are collected in Tables 2 and 4 include an estimate of uncertainties from hadronization globally quoted, together with an estimate of pile-up and underlying-event effects, as uncertainty from non-perturbative sources.

In this context, it should also be mentioned that implementing b -quark initiated processes in NLO QCD Monte-Carlo event generators still presents some issues. We discussed in Section 2.1 how radiative corrections to tree-level b -initiated processes includes processes involving only light quarks in the initial state and b quarks in the final state (e.g.: $gg \rightarrow b\bar{b}\gamma$ is an $O(\alpha_s)$ real-emission correction to $bg \rightarrow b\gamma$). In order to automatically generate the radiative-correction processes from the corresponding tree-level process, the b quark should be consistently treated as massless or massive in both the initial and final state. Therefore, the traditional 5F prescription of considering a b quark as massless in b -initiated processes and massive when it only enters as a final-state parton (the so called S-ACOT scheme⁵⁹) might be impractical, if not inconsistent, in the context of a NLO QCD event generator. Different implementations of 5F in NLO parton-shower Monte Carlo have considered and partially addressed the problem with different methods, while a more rigorous solution is still being developed.

To clarify this issue, let us observe that the treatment of processes initiated by heavy quarks and the rigorous definition of a heavy-quark parton density has been studied⁶⁰ and there is no conceptual obstacle in considering an initial-state heavy quark as massive. Indeed, a well-defined scheme to build fully-massive heavy-quark PDF have been proposed, the ACOT scheme,⁶¹ and implemented in a few sets of PDF, namely CTEQ4-6(HQ). However, if the heavy-quark PDF is entirely generated via perturbative evolution of gluon and light-quark density, it can be shown⁵⁹ that the problem is equivalent to one in which the initial-state heavy quark is treated as massless and its mass is retained in processes that involve heavy quarks in the final state only. This is clearly very convenient in implementing a 5F calculation, since it allows to treat a large fraction of the contributing subchannels and their loop corrections using a massless heavy quark, greatly simplifying the complexity of the calculation. The corresponding heavy-quark PDF is defined in the S-ACOT scheme,⁵⁹ where the heavy-quark mass (m_b in our case) is kept only as a collinear regulator, and the corresponding collinear logs are resummed using the PDF evolution as reviewed in Section 2.1. Slightly different flavors of the S-ACOT scheme have been implemented in the CTEQ sets of PDF from version 6.5 on.⁶² Other sets of PDF (MSTW, NNPDF) implement slightly different matching schemes (TR^{63,64} for MSTW⁶⁵ and FONNL⁶⁶ for NNPDF⁶⁷) to account for the transition from above to below the heavy-quark mass thresholds, but all rely on the calculation of the b

initiated processes with $m_b = 0$.

Since a consistent implementation of b -initiated processes in a parton-shower NLO Monte Carlo generator naturally call for treating the b quark as massive, one should probably consider adopting the original ACOT scheme and keeping the b -quark mass consistently throughout the calculation. Provided the radiation from initial-state massive quarks is correctly modeled in current NLO Monte-Carlo generators, this will allow accounting for all contributing sub-channels in each $V + b$ -jet process, leaving the mutual balance between them to naturally adapt to the different energy regimes and kinematic regions.

Let us conclude by adding that the incremental reduction of the current main sources of theoretical uncertainty will allow us to consider new level of precision in the future. For instance, there is no estimate at the moment of the effects due to higher-order electroweak (EW) corrections. They are expected to affect the total cross sections by only a few percent, but they might have localized effects on distributions, and will have to be accounted for in the future.

2.3. Photon isolation

We would like to add in this review a special note on the issue of photon isolation, which concerns only the $\gamma + 1b$ -jet and $\gamma + 2b$ -jet processes. Since this issue is often discussed in the corresponding experimental analyses, it is important to clarify the difference yet compatibility between different possible theoretical approaches. We remind the reader that this has been thoroughly discussed in Ref. 9.

Photons in a hadronic environment are usually distinguished into *prompt photons*, when they are directly produced in the hard interaction, and *secondary photons*, when they originate from the hadronization phase of a hadronic jet or the decay of unstable hadrons (e.g. $\pi^0 \rightarrow \gamma\gamma$). While the production of prompt photons can be described in perturbation theory, the production of secondary photons has associated non-perturbative effects that can only be modeled and can therefore introduce a large parametric uncertainty in any given calculation. Since secondary photons tend to preeminently occur in regions of the detector with abundant hadronic activity, in particular within or close to jets, their effect can be eliminated by imposing so-called *isolation cuts* which specifically limit the hadronic activity around a given photon. Prompt photons become then *isolated photons* and can be easily disentangled.

The main theoretical caveat in implementing a given prescription to *isolate* prompt photons from the hard interaction is that such procedure can veto regions of phase space responsible for soft QCD radiation and could therefore spoil the cancellation of infrared divergences between virtual and real corrections in a perturbative QCD calculation. As soon as some residual hadronic activity is admitted in the region around the photon, very energetic collinear final-state partons can produce a small parton-photon invariant mass and the corresponding collinear divergences need therefore to be reabsorbed into suitable non-perturbative fragmentation func-

tions (FF). The cross section for prompt-photon production is then given by,

$$\sigma^\gamma(\mu_R, \mu_F, M_F) = \sigma_{\text{direct}}^\gamma(\mu_R, \mu_F) + \int_0^1 dz \sum_i \sigma_i(\mu_R, \mu_F, M_F) D_{i \rightarrow \gamma}(z, M_F), \quad (5)$$

where $\sigma_{\text{direct}}^\gamma$ represents the cross section for the direct-photon component while σ_i denotes the cross section for the production of a parton i that further fragments into a photon. The fragmentation of a parton i into a photon is represented by the corresponding photon FF, $D_{i \rightarrow \gamma}(z, M_F)$, where z is the fraction of the parton momentum that is carried by the photon, and M_F is the fragmentation scale. Examples of available FF in the literature are by Bourhis, Fontannaz and Guillet (set I and II),⁶⁸ and by Gehrmann-de Ridder and Glover.⁶⁹ Fragmentation functions for final-state partons, like PDF for initial-state partons, are intrinsically non perturbative and introduce into the calculation the same kind of uncertainty in the modeling of secondary photons that one originally wanted to eliminate. How relevant the contribution of fragmentation functions is depends on the chosen isolation prescription.

Theoretical calculations normally use two main prescriptions denoted as *fixed-cone* and *smooth-cone* (or *Frixione*) prescriptions respectively. The *fixed-cone* prescription is commonly used in experiments and limits the hadronic activity inside a cone of radius R_0 around the photon by imposing that the hadronic transverse energy inside the cone does not exceed a maximum value, E_T^{max} , set by the experiment, i.e.

$$\sum_{\in R_0} E_T(\text{had}) < E_T^{\text{max}}, \quad (6)$$

where $R_0 = \sqrt{\Delta\eta^2 + \Delta\phi^2}$, and $\Delta\eta$ and $\Delta\phi$ are the pseudorapidity and azimuthal-angle differences between the photon and any hadronic activity. After the isolation cut, the value of z is typically large, and since the FF are dominant in the low z region, the isolation procedure suppresses the fragmentation contribution substantially.

Alternatively, the *smooth-cone* isolation prescription introduced by Frixione,⁷⁰ limits the hadronic activity around a photon by imposing a threshold on the transverse hadronic energy within a cone about the photon that varies with the radial distance from the photon, i.e

$$\sum_i E_T^i \theta(R - R_{i,\gamma}) < \epsilon E_T^\gamma \left(\frac{1 - \cos R}{1 - \cos R_0} \right)^n \quad \text{for all } R \leq R_0, \quad (7)$$

where the i summation runs over all final-state partons in the process and $E_T^{i(\gamma)}$ is the transverse energy of the parton (photon). R_0 is the size of the isolation cone, ϵ is an isolation parameter of $O(1)$, the exponent is normally set to $n = 1$ or 2 , and

$$R_{i,\gamma} = \sqrt{(\Delta\eta_{i,\gamma})^2 + (\Delta\phi_{i,\gamma})^2}.$$

The θ -function ensures that the i summation only receives contributions from partons that lie inside the isolation cone. $R = R_{i,\gamma}$ if there is only one parton inside the isolation cone. The r.h.s of Eq. 7 vanishes as $R \rightarrow 0$, thus the collinear configurations are suppressed while soft radiation is allowed to be present arbitrarily close to the photon. Since the collinear configurations are completely removed, there is no fragmentation component in Eq. 5.

The fragmentation contribution in the $pp(p\bar{p}) \rightarrow b\bar{b}\gamma$ calculation is included at $O(\alpha\alpha_s^2)$. Due to the photon-isolation requirement, a photon cannot fragment from the tagged b/\bar{b} quark. In the $\gamma + 2b$ case, the photon can only fragment off a light parton j , i.e. σ_i in Eq. 5 is the cross section for the $pp(p\bar{p}) \rightarrow b\bar{b}j$ process calculated at LO, ($\sigma_i = \sigma_{LO}(pp(p\bar{p}) \rightarrow b\bar{b}j)$). We notice that $\sigma_{LO}(pp(p\bar{p}) \rightarrow b\bar{b}j)$ is finite since we impose a cut on the photon transverse momentum. For the $1b$ -tag case, in addition to the same contribution present in the $2b$ -tag case, the photon can also fragment off an unidentified b/\bar{b} quark. The LO $pp(p\bar{p}) \rightarrow b\bar{b}j$ cross section is divergent in this case since the light parton in the final state can be soft and/or collinear. To overcome this problem, one should start from the $pp(p\bar{p}) \rightarrow b\bar{b}$ cross section at NLO in QCD. We also notice that when the photon is fragmented off of a b/\bar{b} quark, terms proportional to $\ln(M_F^2/m_b^2)$, arising from the collinear configuration of the $b \rightarrow b\gamma$ splitting in the (direct) $pp(p\bar{p}) \rightarrow b\bar{b}\gamma$ process, have to be subtracted to avoid double counting since those terms have been included and resummed in the b quark-to-photon fragmentation function via DGLAP evolution equations.

Having implemented both methods in $\gamma + 2b$ production, very little if no difference was found in Ref. 9. Similar conclusions have been reached in other studies involving the associated production of a photon and several jets.^{71,72} This should be emphasized to the benefit of the experimental measurements, since the experimental set up (where energy depositions are intrinsically discretized) only allows for a *fixed-cone* isolation criterion (while the *smooth-cone* criterion is a continuous prescription, even if discrete versions can be explored).

3. Experimental Measurements and Theory Predictions

Experimental measurements of vector-boson production in association with b jets started^d in 2008³⁶ and has been followed by more recent studies by all the major high-energy-physics experimental collaborations:

- $W + b$ jets by CDF,³³ ATLAS,^{41,42} D0,^{34,35} and CMS;⁴³
- $Z + b$ jets by CDF,³⁶ ATLAS,^{44,45} CMS^{46–48} and D0;³⁷
- $\gamma + b$ jets by D0,^{39,40} and CDF.³⁸

More activity is expected in the near future, since, for instance, all the studies published so far by the LHC collaborations have been based on $\sqrt{s} = 7$ TeV data samples only. With the larger datasets collected in Run I of the LHC at $\sqrt{s} = 8$ TeV

^dWe also note the earlier measurement in Ref. 73 of the $\sigma(p\bar{p} \rightarrow Z + b\text{jet})/\sigma(p\bar{p} \rightarrow Z + \text{jet})$ ratio.

and expected in Run II at or above $\sqrt{s} = 13$ TeV, new possibilities will open and new challenges will be met, such that more accurate measurements will become available.

One central and common feature of all measurements mentioned is the need for b -jet tagging algorithms. The main characteristic for tagging b jets is of course the presence of a secondary vertex in the related jet. In order to increase the purity of the samples, other requirements can be imposed on, for instance, the tagging of decay products of the associated meson (typically leptons), or the impact parameters, invariant mass, and number of tracks associated with the secondary vertex. All these variables are combined in multivariate analyses. In the end the experiments report b -jet tagging efficiencies between 35% and 50%, considerably lower than b -tagging efficiencies around 85% reported, for instance, in studies of $t\bar{t}$ production (see for example Ref. 74). Indeed one must observe that, with the tagging algorithms employed in $V+b$ -jet analyses, light-jet mistag rates are actually very low, at the per-mille level for light jets and at the few-percent level for c jets. This is necessary when studying $V+b$ jet signals, since much lower jet multiplicities are explored compared to $t\bar{t}$ studies. Unlike $t\bar{t}$ production, where one can also exploit kinematical constraints to exclude signals from light QCD jets, $V+b$'s signatures can be overwhelmed by backgrounds like $V+1$ light-jet with the light jet misidentified as a b jet. The net effect is that a high-purity b -tagging algorithm has a reduced efficiency.

An important issue in b -jet tagging is the possibility of constraining the number of B hadrons in the tagged jet. Many of the algorithms employed so far look for jets that contain a B hadron, in principle associated with a b quark from the original hard interaction. But it has been observed that care must be taken with jets that contain pairs of B hadrons which can be associated with a gluon splitting into an almost collinear $b\bar{b}$ pair. These jets are called *merged b jets* and denoted as (bb) jets. Contributions of (bb) jets in studies of signatures with b jets can be seen as reducible backgrounds. From the theoretical side, it is known that gluon splitting into heavy quarks needs special attention and improved modeling in parton showers (see discussion in Section 2). Strategies to reduce these backgrounds are then advantageous. In particular, studies like the one presented by ATLAS in Ref. 56, where techniques were developed to tag (bb) jets, are very important. ATLAS indeed found that they could develop algorithms to reject (bb) jets at the 95% level, while retaining b jets with a 50% efficiency. We notice that this latter study shows that a measurement on merged b jets is possible, a result that should be of great interest to the theory community that wants to improve the description of $g \rightarrow b\bar{b}$ splitting in parton showers.

In the following subsections we review the most recent experimental measurements of $V+b$ jets ($V = W^\pm, Z/\gamma^*, \gamma$) and highlight the comparisons to theoretical predictions that have been reported in the corresponding experimental papers. In Section 3.1 we present results for $W+b$ -jet production, in Section 3.2 for Z/γ^*+b -jet production, and in Section 3.3 for $\gamma+b$ -jet production. We do not present all the

details of the experimental analyses, but limit ourselves to show tables and plots that well capture and summarize the main features of these studies with particular emphasis on those aspects that have a direct influence on the comparison with theoretical predictions. In particular, Tables 1, 3, and 5 present a synopsis of the experimental set up for each analysis. In the first column we give the experiment (first the Tevatron experiments, CDF and D0, followed by the LHC experiments, ATLAS and CMS), the center-of-mass energy, the data set used, and the paper from where the results have been taken. In the second column we list the signatures that have been selected by each experiment, and in this context we denote by b a b jet and by j a light jet, while we denote inclusive measurements (usually denoted in the experimental papers by *at least one b jet* or *at least one b and one light jet* or similar) adding a $+X$ to the main jet signature. Finally, in the third column we report the detailed kinematical cuts and vetos employed at the particle level, which should directly correspond to what has been used in obtaining the corresponding theoretical predictions. Experimental results and theoretical predictions for total cross sections (and ratios of) are listed in Tables 2 and 4. We have extracted the theoretical results from the corresponding experimental papers, and therefore they are not often directly comparable among themselves since they might correspond to different set ups and different calculations. We will highlight these differences in the discussion and emphasize what we can learn from the comparison. We will also include several figures from different studies to illustrate the comparison between experimental measurements and theoretical predictions of total and differential cross sections

3.1. Measurements of W hadronic production in association with b jets

All studies presented for $W + b$ -jet hadronic production consider leptonic decays of the W boson, employing either the electron channel ($W \rightarrow e\nu_e$) or the muon channel ($W \rightarrow \mu\nu_\mu$) or both, while the decay into a tau lepton is considered as a background. Consequently the signatures studied contain missing transverse energy, \cancel{E}_T , due to the transverse momentum of the escaping neutrino, p_T^ν . This \cancel{E}_T is measured in the detectors by adding (vectorially in the transverse plane) energy depositions around the detector. In theory calculations such \cancel{E}_T is identified with p_T^ν , which in experimental measurements can not directly be measured. In what follows we choose to always write \cancel{E}_T while quoting kinematical cuts for the different experimental studies, as missing transverse energy is the fundamental object that can be studied experimentally.^e

The main backgrounds that affect the $W(\rightarrow l\nu_l) + b$ -jet signatures are: $W + c$ jets and W +light jets where one (or more) jet(s) is mistagged as a b -jet; $t\bar{t}$ and single-top

^eWe do this in spite of the fact that all the experimental studies use p_T^ν in constraining different signatures, because we think it is more appropriate. In fact, it would be better to identify \cancel{E}_T with the negative sum of the momenta of the observed jets (light or heavy) in the transverse plane.

production; and multijet production (with some of the light jet mimicking leptons). Also Drell-Yan processes (with extra light jets) and diboson production can have relevant contributions as backgrounds. Kinematical cuts and vetos are often applied to minimize background, for example in extra leptons or jets to avoid contamination from top-pair production.

Table 1. $W + b$ -jet experimental signatures and kinematics from all major high-energy-physics experiments. Details are presented in the text.

Experiment	Signatures	Kinematics
CDF, ³³ 1.96 TeV, 1.9 fb ⁻¹	$W(\rightarrow l\nu_l) + b$ $W(\rightarrow l\nu_l) + b + j$ $W(\rightarrow l\nu_l) + b + b$	$p_T^l > 20$ GeV, $ \eta^l < 1.1$, $\cancel{E}_T > 25$ GeV <i>Jets:</i> Cone-based algorithm, $R = 0.4$ $E_T^j > 20$ GeV, $ \eta^j < 2$
D0, ³⁴ 1.96 TeV, 6.1 fb ⁻¹	$W(\rightarrow l\nu_l) + b + X$	<i>Muon channel:</i> $p_T^\mu > 20$ GeV, $ \eta^\mu < 1.7$, <i>Electron channel:</i> $p_T^e > 20$ GeV, $ \eta^e < 1.1$, or $1.5 < \eta^e < 2.5$ $\cancel{E}_T > 25$ GeV <i>Jets:</i> Midpoint algorithm, $R = 0.5$ $p_T^b > 20$ GeV, $ \eta^b < 1.1$
ATLAS, ⁴² 7 TeV, 4.6 fb ⁻¹	$W(\rightarrow l\nu_l) + b$ $W(\rightarrow l\nu_l) + b + j$ $W(\rightarrow l\nu_l) + b + b$	$p_T^l > 25$ GeV, $ \eta^l < 2.5$, $\cancel{E}_T > 25$ GeV, $M_T^W > 60$ GeV <i>Jets:</i> Anti- k_T algorithm, $R = 0.4$ $p_T^j > 25$ GeV, $ y^j < 2.1$ $\Delta R(l, j) > 0.5$
CMS, ⁴³ 7 TeV, 5.0 fb ⁻¹	$W(\rightarrow \mu\nu_\mu) + b + b$	$p_T^\mu > 25$ GeV, $ \eta^\mu < 2.1$, $\cancel{E}_T > 25$ GeV <i>Jets:</i> Anti- k_T algorithm, $R = 0.5$ $p_T^b > 25$ GeV, $ \eta^b < 2.4$ <i>Jet Veto:</i> $p_T^j > 25$ GeV, $ \eta^j < 4.5$

3.1.1. *Experimental setups and total cross sections*

In Tables 1 and 2 we present a detailed account of the most recent studies of each of the major high-energy-physics experimental collaborations for $W + b$ -jets hadronic production.

Experimental details are shown in Table 1. In the *signature* column we show the lepton channels employed, either $W(\rightarrow e\nu_e)$ or $W(\rightarrow \mu\nu_\mu)$ for the electron or muon channel respectively, and when these are combined we write $W(\rightarrow l\nu_l)$. Notice that tau decays are actually considered as background and no hadronic decay mode is considered since they are affected by large backgrounds. We pay special attention to

the jet multiplicity and, using the notation explained at the beginning of this section, we distinguish between exclusive and inclusive ($\dots + X$) measurement and we specify how many b jets and light jets are part of the signature. This is very important in understanding the comparison with theory. The kinematical cuts shown in Table 1 define the phase space considered to produce theoretical predictions at the particle level. We note that experimental analyses use more sophisticated selections, tailored to the optimization of the experimental apparatus and the available data, and subsequently *transform* these, via an *unfolding* procedure, to a set of simpler cuts and vetos to be used in theory Monte Carlo generators. Care must be taken to reduce as much as possible the unfolding procedure in order to minimize the sensitivity to the modeling of data in the Monte Carlo employed by the experiment.

Table 2. $W + b$ -jet measurements by the major high-energy-physics experiments and corresponding theoretical predictions. The CDF measurement corresponds to a jet cross section, while all others are event cross sections. Details are presented in the text.

Setup	Cross sections in pb		
CDF ³³	Experiment	2.74	$\pm 0.27(\text{stat.}) \pm 0.42(\text{syst.})$
	Theory	1.22	$\pm 0.14(\text{scale})$
D0 ³⁴	Experiment (<i>Muon channel</i>)	1.04	$\pm 0.05(\text{stat.}) \pm 0.12(\text{syst.})$
	Theory (<i>Muon channel</i>)	1.34	$^{+0.40}_{-0.33}(\text{scale}) \pm 0.06(\text{PDF})^{+0.09}_{-0.05}(m_b)$
	Experiment (<i>Electron channel</i>)	1.00	$\pm 0.04(\text{stat.}) \pm 0.12(\text{syst.})$
	Theory (<i>Electron channel</i>)	1.28	$^{+0.40}_{-0.33}(\text{scale}) \pm 0.06(\text{PDF})^{+0.09}_{-0.05}(m_b)$
	Experiment (<i>Combined</i>)	1.05	$\pm 0.03(\text{stat.}) \pm 0.12(\text{syst.})$
	Theory (<i>Combined</i>)	1.34	$^{+0.40}_{-0.33}(\text{scale}) \pm 0.06(\text{PDF})^{+0.09}_{-0.05}(m_b)$
ATLAS ⁴²	Experiment (1 jet)	5.0	$\pm 0.5(\text{stat.}) \pm 1.2(\text{syst.})$
	Theory (1 jet)	3.01	$\pm 0.07(\text{stat.})^{+0.72}_{-0.54}(\text{scale}) \pm 0.04(\text{PDF})$ $\pm 0.08(\text{NP})^{+0.40}_{-0.29}(\text{DPI})$
	Experiment (2 jets)	2.2	$\pm 0.2(\text{stat.}) \pm 0.5(\text{syst.})$
	Theory (2 jets)	1.69	$\pm 0.06(\text{stat.})^{+0.40}_{-0.23}(\text{scale}) \pm 0.04(\text{PDF})$ $\pm 0.08(\text{NP})^{+0.12}_{-0.09}(\text{DPI})$
	Experiment (1 or 2 jets)	7.1	$\pm 0.5(\text{stat.}) \pm 1.4(\text{syst.})$
	Theory (1 or 2 jets)	4.70	$\pm 0.09(\text{stat.})^{+0.60}_{-0.49}(\text{scale}) \pm 0.06(\text{PDF})$ $\pm 0.16(\text{NP})^{+0.52}_{-0.38}(\text{DPI})$
CMS ⁴³	Experiment	0.53	$\pm 0.05(\text{stat.}) \pm 0.09(\text{syst.}) \pm 0.06(\text{theo.}) \pm 0.01(\text{lumi.})$
	Theory	0.55	$\pm 0.03(\text{scale}\&\text{PDF}) \pm 0.01(\text{NP}) \pm 0.05(\text{DPI})$

The results of the measurements introduced in Table 1 are shown in Table 2, where we also collect some of the theoretical predictions quoted by the experimental papers. CDF reports jet cross sections, while all other experiments give event cross sections. We present the full set of reported uncertainties. For experimental results these are of statistical and systematic nature. Also, CMS separate the uncertainty due to Monte Carlo modeling in the extraction of selection efficiencies (“theo.”) and the one due to luminosity determination. Experimental statistical uncertainties are relatively low, of the order of 10%, for all measurements. It is to be expected that statistical errors at the total-cross-section level will be relatively marginal for all

future LHC studies (either at $\sqrt{s} = 8$ TeV or at $\sqrt{s} = 13$ TeV). The challenge for the experiments will then be to reduce systematic uncertainties (which so far vary between 10% and 30%) through a better understanding of their detectors. In particular, reducing the systematic uncertainty associated to b -jet tagging procedures might be crucial. For ATLAS and CMS, the larger luminosity environment of RUN II, with the larger number of pile-up events, will pose serious difficulties.

The theory predictions listed in Table 2 are all parton-level predictions that include NLO QCD corrections as implemented in MCFM following Refs. 5, 27, 7, 28. In the ATLAS and CMS studies, they have been corrected by non-perturbative effects. The theoretical uncertainty is separated in: dependence on the (unphysical) factorization and renormalization scales (“scale”), dependence on the choice of parton distribution functions (“PDF”), dependence on the value of m_b , non-perturbative corrections (“NP”), and dependence on the modeling of contributions from double-parton interactions (“DPI”).

All theory results show a relatively large unphysical scale sensitivity around 15% to 30%. Although a full calculation of Next-to-Next-to-Leading-Order (NNLO) QCD corrections might be far in the future, it might be possible to compute the gauge-invariant pieces most sensitive to scale variations. It has been noticed that this sensitivity comes mainly from the tree-like NLO QCD real corrections associated to a quark-gluon initial state. A step towards this has been achieved by computing 1-loop amplitudes for $Wb\bar{b}j$,²⁶ and even more in Ref. 25 where full NLO QCD corrections have been computed. We notice that CMS, which has presented a measurement for the exclusive $W + b + b$ process, has estimated the scale sensitivity following the prescription of Ref. 75. This is a way to give a more meaningful theoretical scale uncertainty since, for exclusive processes, the dependence on the scale variation tends to be relatively small (given the reduced impact from tree-like real contributions^{5,6}). PDF uncertainties are mild and of the order of 2% to 4%. Non-perturbative uncertainties are mainly associated to hadronization and underlying-event models. ATLAS calculates them using the implementation of $Wb\bar{b}$ production in POWHEG BOX, which however is a purely 4F calculation and might not give the correct information for $W + b + X$ (while it would for $W + b + b$ or $W + b + b + X$). CMS, on the other hand, estimates hadronization corrections comparing with a tree-level simulation obtained using MadGraph+PYTHIA. Since CMS measured a $W + b + b$ cross section, using the aforementioned implementation in POWHEG BOX or in any other NLO parton-shower Monte Carlo generator (as mentioned in the introduction, $Wb\bar{b}$ is also available e.g. in MadGraph5_aMC@NLO) would have provided a more adequate information. In future predictions we cannot but recommend the systematic use of NLO QCD parton-shower Monte Carlo generators to directly assess the impact of these non-perturbative effects. Finally it is important to mention the large theory uncertainty quoted by ATLAS and CMS as due to double-parton interactions (DPI). ATLAS estimates that double-parton interaction has a large impact, of the order of 25%, on the total cross section, while CMS accounts for an effect at the

15-10% level. Even more, ATLAS shows that, when quoted differentially in b -jet p_T , these contribution mostly fall in the lower bins. It is interesting to notice that, as we will see in Section 3.2, the contribution of DPI to the $Z/\gamma^* + b$ -jet cross section is estimated by CMS to be below 5%,⁴⁸ also occurring mainly in the lower bins in p_T^b . This difference might be due to the better kinematical resolution achieved via the decaying products of the Z/γ^* boson ($Z/\gamma^* \rightarrow \bar{l}l$ as opposed to $W \rightarrow l\nu_l$) which allows a better modeling of DPI. Given the theoretical challenge involved in rigorously describing DPI in QCD, more dedicated (data driven) studies are needed, in order to be able to reduce the DPI impact on $W + b$ -jet measurements.

Finally in Figure 3 we present a plot with a full account of the ATLAS measurements, including, on top of the NLO QCD predictions of Ref. 28 (MCFM 4FNS+5FNS) other Monte-Carlo-based theory predictions: POWHEG+Pythia, based on the 4F calculation of $Wb\bar{b}$ but matched to a parton shower at NLO in QCD,²⁴ and ALPGEN+Herwig, matched to parton shower but without full NLO QCD corrections. Also, results are reported in jet-multiplicity bins and offer the possibility to assess separately the comparison between theory and experiments in each case.

Looking at the results in Table 2 and Figure 3, one can see that the agreement between experiments and theory is relatively good, although within still sizable uncertainties. We notice that the agreement is definitely better for signatures with at least two jets. For single- b -jet signatures, CDF does have a large excess with significance around 3σ . On the other hand, D0 does not see such discrepancy, but it is important to notice that the measurement by D0 is fully inclusive and it is an event cross section. Also, given the difference in their (both IR unsafe) jet algorithms, the comparison is difficult. On their side, ATLAS measurements are higher than the corresponding theory predictions, but with little significance (around 1.5σ). It will be interesting to see if such tension persists when ATLAS publishes updates with larger data sets. The comparison between different theoretical predictions given in Figure 3, with and without parton-shower and non-perturbative effects, shows clearly that different theoretical estimates are in relatively good agreement, giving confidence in particular in the quoted NLO uncertainty bands. Finally, we note that the slight experimental excess is shown clearly to come from the 1-jet bin. This seems to be confirmed by the complementary CMS measurement which focus on the $W + b + b$ signature, and find excellent agreement between theory and experiment.

3.1.2. Differential cross sections

In order to show how well experiments and theory compare over phase space, we show in Figure 4 a couple of plots from ATLAS⁴² and D0.³⁵ Notice that the differential cross section from D0 comes from a more recent study as compared to the one quoted in Table 1.

Looking at the ATLAS differential cross section as a function of b -jet p_T it seems that the theory predictions deviate considerably from data at large transverse

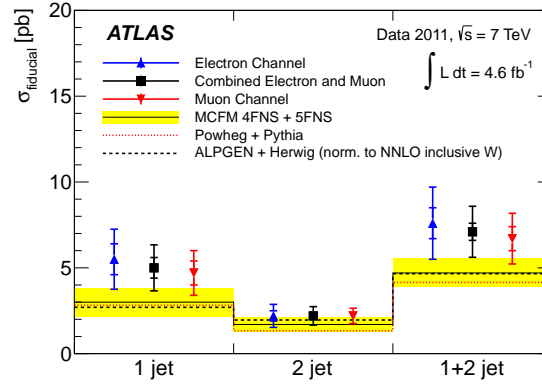


Fig. 3. Total cross sections for $W + b$ -jet hadronic production measured by ATLAS⁴² and compared to theoretical predictions.

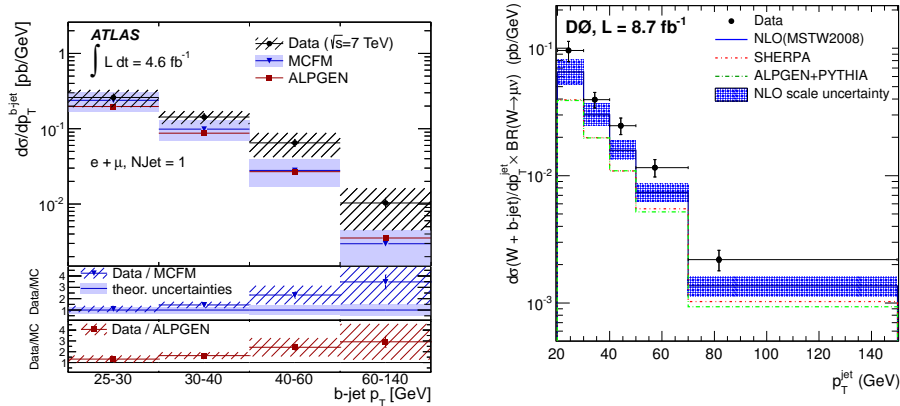


Fig. 4. Differential cross sections for various $W + b$ -jet signatures, as a function of the b -jet p_T , measured by ATLAS⁴² (l.h.s.) and D0³⁵ (r.h.s.), and compared to theoretical predictions.

momentum, where, however, uncertainties are also bigger. On the other hand, the D0 spectrum seems systematically higher with respect to the theoretical predictions, although the ratio between theory and data seems constant. It will be interesting to study these differential distributions more in detail with future larger data sets, and assess the impact of DPI in various p_T^b regions, as first studied by ATLAS⁴² as well as the possibility that large p_T^b bins might be “polluted” by (bb) jets, i.e. jets that contain a pair of B mesons.

3.2. Measurements of Z/γ^* hadronic production in association with b jets

Measurements presented for $Z/\gamma^* + b$ -jet production have employed both electron and muon channels for the decay of the intermediate neutral gauge boson ($Z/\gamma^* \rightarrow e^+e^-, \mu^+\mu^-$). Therefore the main signal consists of a pair of opposite-sign leptons and associated b and light jets.^f The main backgrounds in these studies are represented by top-quark pair production, W production with jets, Z production with light jets, inclusive Z production with Z decaying into tau leptons, diboson and single-top production. In order to enhance the signal, experimentalists choose kinematical cuts and apply vetos as needed.

Table 3. $Z/\gamma^* + b$ -jet experimental signatures and kinematics from all major high-energy-physics experiments. Details are presented in the text.

Experiment	Signatures	Kinematics
CDF, ³⁶ 1.96 TeV, 2 fb ⁻¹	$Z/\gamma^*(\rightarrow l\bar{l}) + b + X$	$76 \text{ GeV} < M_{ll} < 106 \text{ GeV}$ Jets: Cone-based algorithm, $R = 0.7$ $E_T^b > 20 \text{ GeV}$, $ \eta^b < 1.5$
D0, ³⁷ 1.96 TeV, 9.7 fb ⁻¹	$\left(\frac{Z/\gamma^*(\rightarrow l\bar{l})+b+X}{Z/\gamma^*(\rightarrow ll)+j+X}\right)$	$70 \text{ GeV} < M_{ll} < 110 \text{ GeV}$ Muon channel: $p_T^{1st \mu} > 15 \text{ GeV}$, $p_T^{2nd \mu} > 10 \text{ GeV}$, $ \eta^\mu < 2$ Electron channel: $p_T^e > 15 \text{ GeV}$, $ \eta^e < 1.1$, or $1.5 < \eta^e < 2.5$, Jets: Midpoint algorithm, $R = 0.5$ $p_T^b > 20 \text{ GeV}$, $ \eta^b < 2.5$
ATLAS, ⁴⁵ 7 TeV, 4.6 fb ⁻¹	$Z/\gamma^*(\rightarrow l\bar{l}) + b + X$ $Z/\gamma^*(\rightarrow ll) + b + b + X$	$p_T^l > 20 \text{ GeV}$, $ \eta^l < 2.5$, $76 \text{ GeV} < M_{ll} < 106 \text{ GeV}$ Jets: Anti- k_T algorithm, $R = 0.4$ $p_T^j > 20 \text{ GeV}$, $ y^j < 2.4$ $\Delta R(l, j) > 0.5$
CMS, ⁴⁸ 7 TeV, 5.0 fb ⁻¹	$Z/\gamma^*(\rightarrow l\bar{l}) + b$ $Z/\gamma^*(\rightarrow ll) + b + X$ $Z/\gamma^*(\rightarrow ll) + b + b + X$	$p_T^l > 20 \text{ GeV}$, $ \eta^l < 2.4$, $76 \text{ GeV} < M_{ll} < 106 \text{ GeV}$ Jets: Anti- k_T algorithm, $R = 0.5$ $p_T^j > 25 \text{ GeV}$, $ \eta^j < 2.1$ $\Delta R(l, j) > 0.5$

^fThis signature can be generated by both Z and γ^* although the first component is largely dominant.

3.2.1. *Experimental setups and total cross sections*

In Table 3 we present details of the experimental setups employed on $Z + b$ -jet production studies, using the same format of Table 1. Unlike the case of $W + b$ -jet measurements, most of the results shown here are inclusive in the number of jets. Also, as it is needed in order to avoid the massless photon pole, a cut on the invariant mass of the lepton pair is always imposed around the Z peak.

Table 4. $Z/\gamma^* + b$ -jet measurements by the major high-energy-physics experiments and corresponding theoretical predictions. CDF and D0 measurements are ratio of cross sections. Details are presented in the text.

Setup	Cross sections or ratios		
CDF ³⁶	Experiment (ratio to inclusive Z)	$(3.32 \pm 0.53(\text{stat.}) \pm 0.42(\text{syst.})) \times 10^{-3}$	
	Theory (ratio to inclusive Z)	$(2.3 - 2.8)(\text{scale}) \times 10^{-3}$	
D0 ³⁷	Experiment (ratio)	$0.0196 \pm 0.0012(\text{stat.}) \pm 0.0013(\text{syst.})$	
	Theory (ratio)	$0.0206^{+0.0022}_{-0.0013}(\text{scale\&NP})$	
ATLAS ⁴⁵	Experiment [fb] (at least 1 b jet)	4820	$\pm 60(\text{stat.})^{+360}_{-380}(\text{syst.})$
	Theory, MCFM [fb] (at least 1 b jet)	5230	$\pm 30(\text{stat.})^{+690}_{-710}(\text{scale\&NP})$ $\pm 6\%(\text{PDF})$
	Theory, 4FNS aMC@NLO [fb] (at least 1 b jet)	3390	$\pm 20(\text{stat.})^{+580}_{-480}(\text{scale})$
	Theory, 5FNS aMC@NLO [fb] (at least 1 b jet)	4680	$\pm 40(\text{stat.})^{+550}_{-580}(\text{scale})$
	Experiment [fb] (at least 2 b jets)	520	$\pm 20(\text{stat.})^{+74}_{-72}(\text{syst.})$
	Theory, MCFM [fb] (at least 2 b jets)	410	$\pm 10(\text{stat.})^{+60}_{-60}(\text{scale\&NP})$ $\pm 5\%(\text{PDF})$
	Theory, 4FNS aMC@NLO [fb] (at least 2 b jets)	485	$\pm 7(\text{stat.})^{+80}_{-70}(\text{scale})$
	Theory, 5FNS aMC@NLO [fb] (at least 2 b jets)	314	$\pm 9(\text{stat.})^{+30}_{-30}(\text{scale})$
CMS ⁴⁸	Experiment [pb] (1 b jet)	3.52	$\pm 0.02(\text{stat.}) \pm 0.20(\text{syst.})$
	Theory, MCFM [pb] (1 b jet)	3.03	$^{+0.30}_{-0.36}(\text{scale})$
	Theory, 4FNS aMC@NLO [pb] (1 b jet)	2.36	$^{+0.47}_{-0.37}(\text{scale})$
	Theory, 5FNS aMC@NLO [pb] (1 b jet)	3.70	$^{+0.23}_{-0.26}(\text{scale})$
	Experiment [pb] (at least 1 b jet)	3.88	$\pm 0.02(\text{stat.}) \pm 0.22(\text{syst.})$
	Theory, MCFM [pb] (at least 1 b jet)	3.23	$^{+0.34}_{-0.40}(\text{scale})$
	Theory, 4FNS aMC@NLO [pb] (at least 1 b jet)	2.71	$^{+0.52}_{-0.41}(\text{scale})$
	Theory, 5FNS aMC@NLO [pb] (at least 1 b jet)	3.99	$^{+0.25}_{-0.29}(\text{scale})$
	Experiment [pb] (at least 2 b jets)	0.36	$\pm 0.01(\text{stat.}) \pm 0.07(\text{syst.})$
	Theory, MCFM [pb] (at least 2 b jets)	0.29	$^{+0.04}_{-0.04}(\text{scale})$
Theory, 4FNS aMC@NLO [pb] (at least 2 b jets)	0.35	$^{+0.08}_{-0.06}(\text{scale})$	
Theory, 5FNS aMC@NLO [pb] (at least 2 b jets)	0.29	$^{+0.04}_{-0.04}(\text{scale})$	

In Table 4 we show the results of the experimental measurements, together with the theoretical predictions quoted by the experimental studies. Notice that, although CDF³⁶ showed results for jet-level cross sections, we show only results for the ratio with respect to inclusive Z -boson production, since this is the observable that they compare to theoretical predictions. Also, as shown in Table 3, D0 measurement is a ratio of event cross sections for inclusive production of $Z + b + X$ and $Z + j + X$. ATLAS and CMS results are event cross sections. For all measurements we present theoretical results based on parton-level calculations that include NLO QCD results.

Also, for ATLAS and CMS we include fully showered results including NLO QCD corrections for the hard interaction, both in the 4F and in the 5F schemes.

Reported errors are of statistical and systematic nature for experimental measurements. For theory, reported errors correspond to statistical integration errors (“stat.”), sensitivity to unphysical renormalization and factorization scales (“scale”), non-perturbative corrections (“NP”), and choice of parton distribution functions (“PDF”). The latter has been estimated only for the ATLAS results, as they report theoretical predictions using three different sets of PDF (MSTW2008,⁷⁶ CT10,⁷⁷ and NNPDF23⁷⁸).

The statistical errors of the experimental measurements are all below 6% except for the CDF result, which happens to use a fraction of their final data set. All systematic errors are relatively small, below 14% (except for the inclusive two b -jet measurement from CMS, which has 19%). Theoretical uncertainties tend to be dominated by a scale sensitivity of the order of 15%, with PDF uncertainties relatively low at the 5% level. ATLAS has included non-perturbative corrections to the parton level NLO QCD results due to DPI, and estimated them to be of order 1%, much smaller than the corresponding corrections in $W + b$ jet production. As we commented in Section 3.1, this may be due to the better resolved kinematics that allows a better and more constrained modeling of $Z/\gamma^* + b$ -jets DPI contributions.

Both ATLAS and CMS have included comparisons to theoretical results based on parton showers that consistently include NLO QCD corrections for the hard interaction. A summary at a glance of the ATLAS study for both $Z/\gamma^* + b + X$ and $Z/\gamma^* + 2b + X$ signatures is nicely illustrated in Figure 5. This is an important step, as we hope in the future to be able to consistently study all observables including quantum corrections fully showered and hadronized to reach hadron level predictions. Even more, when analyzing signatures with multiple jet bins, techniques for merging NLO QCD matrix elements for different multiplicities can be employed.⁷⁹ Doing this one has a proper way of comparing theoretical results (with well estimated uncertainties) directly with the observables measured by the experiments. In particular, both ATLAS and CMS have employed the aMC@NLO framework. In the future, it will be relevant to systematically compare predictions using other NLO QCD parton-shower Monte Carlo, such as the POWHEG BOX and SHERPA.

Comparing experimental measurements to the corresponding theoretical results obtained at NLO QCD or adding parton shower, in the 4F and 5F schemes, one can notice that shower and hadronization effects (not included in the CMS results from MCFM) have an impact of the order of 20%. Also, it is clear that the choice of scheme (either 4F or 5F) has a considerable impact at the parton-shower NLO QCD level. For example, it is clear that 5F results compare better with single- b -jet measurements, while 4F results compare best to two- b -jet measurements.

Overall, at the level of total rates the $Z/\gamma^* + b$ -jet signatures have good agreement between theory and experiments, at least when comparing to the proper ordering of the perturbative expansion (4F vs 5F). New studies with larger experimental data sets will help further testing this agreement, with particular attention to certain

features that appear over phase space as we will show in the following subsection.

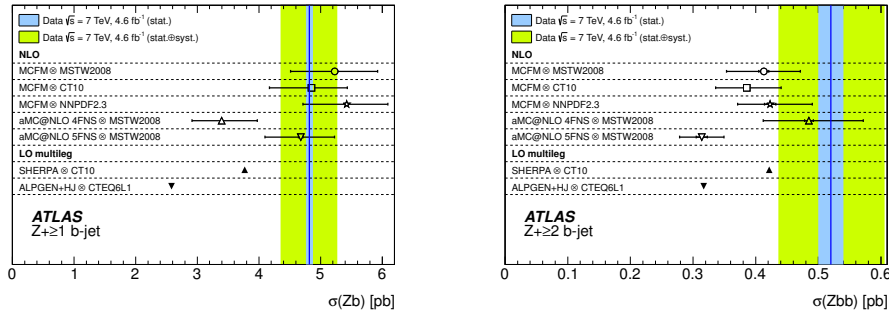


Fig. 5. Total cross sections for hadronic production of $Z/\gamma^* + \geq 1b$ jet and $Z/\gamma^* + \geq 2b$ jets from ATLAS⁴⁵ compared to various theoretical predictions. See text for more details.

3.2.2. Differential cross sections

In Figure 6 we have included several plots of differential cross-section measurements. On the top left, we show a plot from CDF³⁶ for $Z/\gamma^* + b\text{-jet} + X$ production as a function of the transverse momentum of the lepton pair (labeled as p_T^Z). On the top right we show a plot from ATLAS⁴⁵ for $Z/\gamma^* + 2b\text{-jet} + X$ production as a function of the R separation between the b jets. Finally, on the bottom, we show two plots from CMS as published in Ref. 47. As CMS⁴⁸ did not show differential cross section, we have chosen to show the ones in CMS,⁴⁷ which is a study of the associated production of a Z boson and two B mesons. We do not include plots from D0³⁷ because they only show ratios to $Z/\gamma^* + \text{light jet}$ production.

In general the agreement between theory and experiments on all plots in Figure 6 is relatively good. In the ATLAS plot for $Z/\gamma^* + 2b + X$ we notice the poor agreement between the 5F predictions and data, confirming what previously observed for the total cross section, i.e. that 5F is not expected to provide reliable results for processes with two or more b jets (notice that from a parton-shower point of view, this observable is computed at LO). Two of the plots in Figure 6 show distributions for ΔR (for b -jets in the case of ATLAS, and B mesons in the case of CMS) and they both indicate that theoretical descriptions fail to describe the lower bins. A failure to describe the small-angle limit for the production of b jets (hadrons) could be ascribed to badly described gluon splitting into a slightly collinear b -quark pair. One could then correlate these discrepancies with more collinear $g \rightarrow b\bar{b}$ splitting (producing $(b\bar{b})$ jets) which should show up in the tail of distributions in p_T^Z (and also $p_T^{b\text{ jet}}$). Although statistics is poor, there is no evidence of this in the bottom right plot in Figure 6. Future studies might give more hints of correlations between discrepancies for low-angle distributions and large- p_T observables. In the end, this

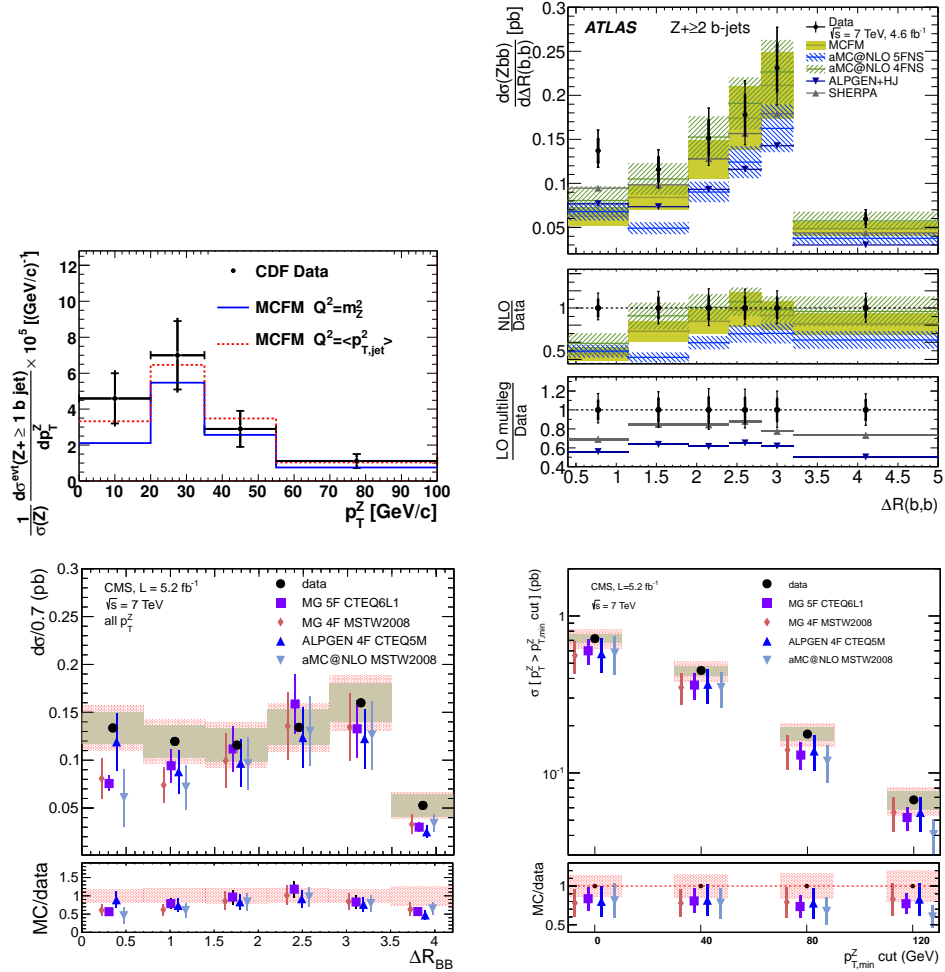


Fig. 6. Differential cross sections from CDF³⁶ (as a function of the transverse momentum of the Z/γ^* boson), ATLAS⁴⁵ (as a function of the R separation between the two b jets) and CMS⁴⁷ (as a function of the R separation of the B hadrons and of the transverse momentum of the Z/γ^* boson) for various $Z/\gamma^* + b$ -jet signatures compared to theoretical predictions.

might point to a poor control of gluon splitting to massive quarks and require better theoretical modeling of (bb) jets.

3.3. Measurements of γ hadronic production in association with b jets

Finally in this subsection we present measurements of the production of a photon γ in association with b jets. Unlike the analyses of the previous section, where the gauge bosons are tagged through their decay to leptons, the photon signatures are

recorded directly through activity in electromagnetic calorimeters. Pollution from signatures that mimic photons, like for example neutral pions decaying into pairs of photons in the electromagnetic calorimeter, have to be dealt with. We show next the measurements presented in the literature by CDF³⁸ and D0.⁴⁰

Table 5. $\gamma + b$ jets: signatures, kinematics.

Experiment	Signatures	Kinematics
CDF, ³⁸ 1.96 TeV, 9.1 fb ⁻¹	$\gamma + b + X$	$E_T^\gamma > 30$ GeV, $ y^\gamma < 1.04$ γ cone isolation ($R = 0.4$): $E_T^{iso} < 2.0$ GeV <hr/> <i>Jets:</i> JETCLU alg., $R = 0.4$ $p_T^j > 20$ GeV, $ y^j < 1.5$ $R_{j,\gamma} > 0.4$
D0, ⁴⁰ 1.96 TeV, 8.7 fb ⁻¹	$\gamma + b + X$ $\gamma + b + b + X$	$p_T^\gamma > 30$ GeV, $ y^\gamma < 1$ or $1.5 < y^\gamma < 2.5$ γ cone isolation ($R = 0.4$): $E_T^{iso} < 2.5$ GeV <hr/> <i>Jets:</i> Midpoint (Run II) alg., $R = 0.5$ $p_T^j > 15$ GeV, $ y^j < 1.5$

3.3.1. *Experimental setups and differential cross sections*

In Table 5 we present the experimental setups of the $\gamma + b$ -jet measurements. Notice that both CDF and DO employ a cone isolation criterion to characterize the (prompt) photon. CDF has considered only the case of central photons ($|y^\gamma| < 1.4$), while D0 has presented results including both central photons ($|y^\gamma| < 1$) and forward photons ($1.5 < |y^\gamma| < 2.5$).

Both CDF and D0 have shown their results differentially as a distribution in the transverse momentum of the photon (p_T^γ). We cannot therefore give a table of results, but will illustrate the comparison between experimental measurements and theory through the p_T^γ distributions themselves. The comparison with the $\gamma + b + X$ measurement of CDF³⁸ is illustrated in Figure 7 while the comparison with both the $\gamma + b + X$ and the $\gamma + b + b + X$ measurements of D0^{39,40} is illustrated in Figures 8 and 9. For the comparison with the $\gamma + b + X$ measurements of both CDF³⁸ and D0³⁹ we show plots from Ref. 9 since they compare to the most up to date theoretical calculations, while for the comparison with the $\gamma + b + b + X$ measurements of D0⁴⁰ we present plots taken from the experimental paper itself where results from Ref. 9 have been used. In Figure 9 data are also compared to results from a LO calculation with p_T -dependent PDF,^{80,81} where however the uncertainty of the prediction is difficult to estimate and to compare with a full NLO calculation using integrated PDF.

It can be appreciated that theory prediction in general describe the data. This is

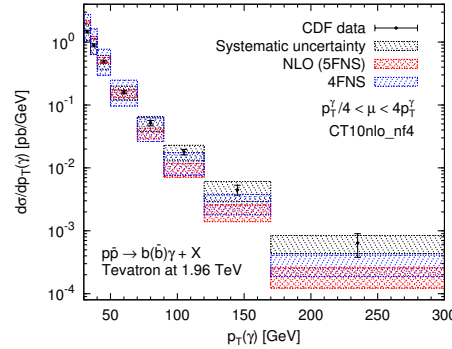


Fig. 7. Differential cross section as a function of p_T^γ measured by CDF³⁸ for $\gamma + b$ -jet production compared to theoretical predictions.⁹

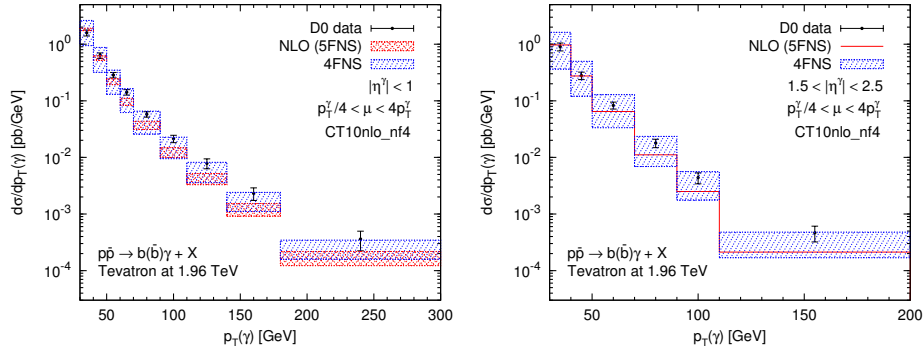


Fig. 8. Differential cross sections as a function of p_T^γ measured by D0³⁹ for $\gamma + b$ -jet production compared to theoretical predictions.⁹

a case even for $\gamma + 1b$ jet, where the 4F prediction is in better agreement with data than the 5F prediction since, as explained in Section 2, the dominant production mode at the Tevatron is via the $q\bar{q}$ channel, which is not influenced by large initial-state logarithms. Still, theory distributions seem slightly softer and fall a little below data at high p_T^γ . Measurements at the LHC will help pushing distributions to much higher p_T^γ and confirm or not these trends. In general there is considerable overlap between 4F and 5F predictions (denoted in the plots by 4FNS and 5FNS) for 1 b -jet observables. As one might expect, from the missing extra b quark, 5F predictions tend to drop faster as a function of the photon transverse momentum.

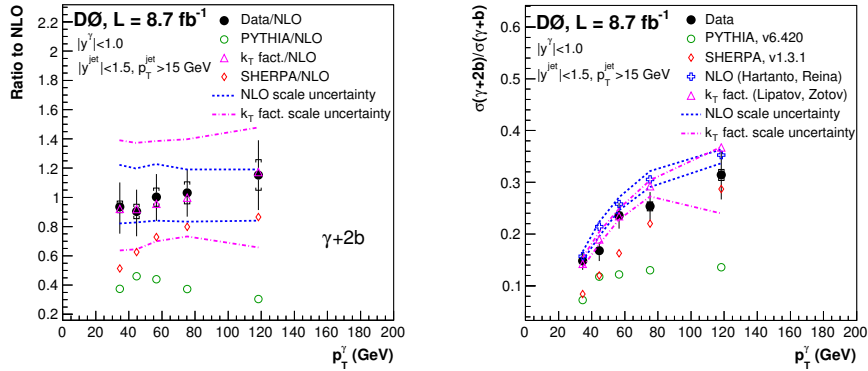


Fig. 9. Ratio of $D0^{40}$ data (and other theory predictions) to NLO QCD prediction (left) for $\gamma + b + b + X$ production, and ratio $(\gamma + 2b + X)/(\gamma + b + X)$ compared to theoretical predictions (right), as a function of p_T^γ .

4. Conclusions

In this review we have presented the current status of electroweak vector-boson associated hadronic production with b jets. Measurements and theoretical predictions for $W + b$ -jet, $Z/\gamma^* + b$ -jet, and $\gamma + b$ -jet signatures were thoroughly reviewed. Results from the major high-energy-physics experimental collaborations, CDF and D0 at the Tevatron, and ATLAS and CMS at the LHC, were summarized.

By now we have reached a mature level in the study of these processes. This is very important given the impact that related studies can have in constraining couplings of the Higgs boson to b quarks, direct studies of heavy-quark parton distribution functions, and searches for new physics.

Although in general we find good agreement between theoretical predictions and experimental measurements, some tensions are still present and important challenges are left for the near future. With the larger data sets collected at $\sqrt{s} = 8$ TeV at the LHC, and with the even larger ones expected at and above $\sqrt{s} = 13$ TeV, we expect improved statistical errors as well as reduced systematic errors (thanks to a better understanding of the detectors). Matching these reduced errors will be challenging for theory predictions. Full parton-showered results, including NLO-QCD corrections and merging prescriptions for different jet multiplicities, as well as systematic studies of hadronization and underlying-event models should become the standard approach. The need for NNLO QCD corrections as well as the inclusion of EW corrections and resummation of large logarithmic corrections could play a role in selected observables and will have to be investigated. More exclusive studies that include larger amount of heavy jets are now also theoretically and experimentally approachable and could lead to better control of the $V + b$ jet processes at hadron

colliders.

Acknowledgments

The Authors would like to thank most of all J. M. Campbell, H. B. Hartanto, and D. Wackerth, with whom many of the studies reviewed in this paper have been completed. The Authors would also like to thank many colleagues on CDF, D0, ATLAS, and CMS, in particular Tobias Golling, Chiara Mariotti, Christopher Neu, Alexander Nikitenko, and Evelyn Thomson, with whom they have enjoyed several fruitful collaborations, and from whom they have learned so many important aspects of the processes presented in this review. The Authors are very grateful to the Aspen Center for Physics for its kind hospitality and support during part of the work that led to this review. F.F.C. has been in part supported by an APS Travel Grant and by the Simons Foundation. The work of F.F.C. is supported by the Alexander von Humboldt Foundation, in the framework of the Sofja Kovalevskaja Award 2014, endowed by the German Federal Ministry of Education and Research. The work of L.R. is partially supported by the U.S. Department of Energy under Grant DE-FG02-13ER41942.

References

1. ATLAS Collaboration, G. Aad *et al.*, *Phys.Lett.* **B716**, 1 (2012), [arXiv:1207.7214 \[hep-ex\]](#).
2. CMS Collaboration, S. Chatrchyan *et al.*, *Phys.Lett.* **B716**, 30 (2012), [arXiv:1207.7235 \[hep-ex\]](#).
3. R. K. Ellis and S. Veseli, *Phys.Rev.* **D60**, 011501 (1999), [arXiv:hep-ph/9810489 \[hep-ph\]](#).
4. J. M. Campbell and R. K. Ellis, *Phys.Rev.* **D62**, 114012 (2000), [arXiv:hep-ph/0006304 \[hep-ph\]](#).
5. F. Febres Cordero, L. Reina and D. Wackerth, *Phys.Rev.* **D74**, 034007 (2006), [arXiv:hep-ph/0606102 \[hep-ph\]](#).
6. F. Febres Cordero, L. Reina and D. Wackerth, *Phys.Rev.* **D80**, 034015 (2009), [arXiv:0906.1923 \[hep-ph\]](#).
7. S. Badger, J. M. Campbell and R. Ellis, *JHEP* **1103**, 027 (2011), [arXiv:1011.6647 \[hep-ph\]](#).
8. F. Febres Cordero, L. Reina and D. Wackerth, *Phys.Rev.* **D78**, 074014 (2008), [arXiv:0806.0808 \[hep-ph\]](#).
9. H. Hartanto and L. Reina, *Phys.Rev.* **D89**, 074001 (2014), [arXiv:1312.2384 \[hep-ph\]](#).
10. J. M. Campbell, R. K. Ellis and C. Williams, Mcfm, from v.7.0 (2015), <http://mcfm.fnal.gov>.
11. J. Alwall, R. Frederix, S. Frixione, V. Hirschi, F. Maltoni *et al.*, *JHEP* **1407**, 079 (2014), [arXiv:1405.0301 \[hep-ph\]](#).
12. T. Gleisberg, S. Hoeche, F. Krauss, M. Schonherr, S. Schumann *et al.*, *JHEP* **0902**, 007 (2009), [arXiv:0811.4622 \[hep-ph\]](#).
13. G. Cullen, H. van Deurzen, N. Greiner, G. Heinrich, G. Luisoni *et al.*, *Eur.Phys.J.* **C74**, 3001 (2014), [arXiv:1404.7096 \[hep-ph\]](#).

32 *Febres Cordero, and Reina*

14. F. Cascioli, P. Maierhofer and S. Pozzorini, *Phys.Rev.Lett.* **108**, 111601 (2012), [arXiv:1111.5206 \[hep-ph\]](#).
15. T. Sjostrand, S. Mrenna and P. Z. Skands, *JHEP* **0605**, 026 (2006), [arXiv:hep-ph/0603175 \[hep-ph\]](#).
16. T. Sjostrand, S. Mrenna and P. Z. Skands, *Comput.Phys.Commun.* **178**, 852 (2008), [arXiv:0710.3820 \[hep-ph\]](#).
17. G. Marchesini, B. Webber, G. Abbiendi, I. Knowles, M. Seymour *et al.*, *Comput.Phys.Commun.* **67**, 465 (1992).
18. G. Corcella, I. Knowles, G. Marchesini, S. Moretti, K. Odagiri *et al.*, *JHEP* **0101**, 010 (2001), [arXiv:hep-ph/0011363 \[hep-ph\]](#).
19. S. Frixione and B. R. Webber, *JHEP* **0206**, 029 (2002), [arXiv:hep-ph/0204244 \[hep-ph\]](#).
20. S. Frixione, P. Nason and B. R. Webber, *JHEP* **0308**, 007 (2003), [arXiv:hep-ph/0305252 \[hep-ph\]](#).
21. R. Frederix, S. Frixione, V. Hirschi, F. Maltoni, R. Pittau *et al.*, *JHEP* **1109**, 061 (2011), [arXiv:1106.6019 \[hep-ph\]](#).
22. P. Nason, *JHEP* **0411**, 040 (2004), [arXiv:hep-ph/0409146 \[hep-ph\]](#).
23. S. Frixione, P. Nason and C. Oleari, *JHEP* **0711**, 070 (2007), [arXiv:0709.2092 \[hep-ph\]](#).
24. C. Oleari and L. Reina, *JHEP* **1108**, 061 (2011), [arXiv:1105.4488 \[hep-ph\]](#).
25. G. Luisoni, C. Oleari and F. Tramontano (2015), [arXiv:1502.01213 \[hep-ph\]](#).
26. L. Reina and T. Schutzmeier, *JHEP* **1209**, 119 (2012), [arXiv:1110.4438 \[hep-ph\]](#).
27. J. M. Campbell, R. K. Ellis, F. Febres Cordero, F. Maltoni, L. Reina *et al.*, *Phys.Rev.* **D79**, 034023 (2009), [arXiv:0809.3003 \[hep-ph\]](#).
28. J. Campbell, F. Caola, F. Febres Cordero, L. Reina and D. Wackerroth, *Phys.Rev.* **D86**, 034021 (2012), [arXiv:1107.3714 \[hep-ph\]](#).
29. J. M. Campbell, R. K. Ellis, F. Maltoni and S. Willenbrock, *Phys.Rev.* **D75**, 054015 (2007), [arXiv:hep-ph/0611348 \[hep-ph\]](#).
30. J. M. Campbell, R. K. Ellis, F. Maltoni and S. Willenbrock, *Phys.Rev.* **D69**, 074021 (2004), [arXiv:hep-ph/0312024 \[hep-ph\]](#).
31. J. M. Campbell, R. K. Ellis, F. Maltoni and S. Willenbrock, *Phys.Rev.* **D73**, 054007 (2006), [arXiv:hep-ph/0510362 \[hep-ph\]](#).
32. T. Stavreva and J. Owens, *Phys.Rev.* **D79**, 054017 (2009), [arXiv:0901.3791 \[hep-ph\]](#).
33. CDF Collaboration Collaboration, T. Aaltonen *et al.*, *Phys.Rev.Lett.* **104**, 131801 (2010), [arXiv:0909.1505 \[hep-ex\]](#).
34. D0 Collaboration Collaboration, V. Abazov *et al.*, *Phys.Lett.* **B718**, 1314 (2013), [arXiv:1210.0627 \[hep-ex\]](#).
35. D0 Collaboration Collaboration, V. M. Abazov *et al.* (2014), [arXiv:1412.5315 \[hep-ex\]](#).
36. CDF collaboration Collaboration, T. Aaltonen *et al.*, *Phys.Rev.* **D79**, 052008 (2009), [arXiv:0812.4458 \[hep-ex\]](#).
37. D0 Collaboration Collaboration, V. M. Abazov *et al.*, *Phys.Rev.* **D87**, 092010 (2013), [arXiv:1301.2233 \[hep-ex\]](#).
38. CDF Collaboration Collaboration, T. Aaltonen *et al.*, *Phys.Rev.Lett.* **111**, 042003 (2013), [arXiv:1303.6136 \[hep-ex\]](#).
39. D0 Collaboration Collaboration, V. Abazov *et al.*, *Phys.Lett.* **B714**, 32 (2012), [arXiv:1203.5865 \[hep-ex\]](#).
40. D0 Collaboration Collaboration, V. M. Abazov *et al.*, *Phys.Lett.* **B737**, 357 (2014), [arXiv:1405.3964 \[hep-ex\]](#).

41. ATLAS Collaboration Collaboration, G. Aad *et al.*, *Phys.Lett.* **B707**, 418 (2012), [arXiv:1109.1470 \[hep-ex\]](#).
42. ATLAS Collaboration Collaboration, G. Aad *et al.*, *JHEP* **1306**, 084 (2013), [arXiv:1302.2929 \[hep-ex\]](#).
43. CMS Collaboration Collaboration, S. Chatrchyan *et al.*, *Phys.Lett.* **B735**, 204 (2014), [arXiv:1312.6608 \[hep-ex\]](#).
44. ATLAS Collaboration Collaboration, G. Aad *et al.*, *Phys.Lett.* **B706**, 295 (2012), [arXiv:1109.1403 \[hep-ex\]](#).
45. ATLAS Collaboration Collaboration, G. Aad *et al.*, *JHEP* **1410**, 141 (2014), [arXiv:1407.3643 \[hep-ex\]](#).
46. CMS Collaboration Collaboration, S. Chatrchyan *et al.*, *JHEP* **1206**, 126 (2012), [arXiv:1204.1643 \[hep-ex\]](#).
47. CMS Collaboration Collaboration, S. Chatrchyan *et al.*, *JHEP* **1312**, 039 (2013), [arXiv:1310.1349 \[hep-ex\]](#).
48. CMS Collaboration Collaboration, S. Chatrchyan *et al.*, *JHEP* **1406**, 120 (2014), [arXiv:1402.1521 \[hep-ex\]](#).
49. F. Maltoni, G. Ridolfi and M. Ubiali, *JHEP* **1207**, 022 (2012), [arXiv:1203.6393 \[hep-ph\]](#).
50. R. Barnett, H. Haber and D. Soper, *Nucl. Phys.* **B306**, 697 (1988).
51. F. Olness and W.-K. Tung, *Nucl. Phys.* **B308**, 813 (1988).
52. D. Dicus, T. Stelzer, Z. Sullivan and S. Willenbrock, *Phys. Rev.* **D39**, 751 (1989).
53. V. Gribov and L. Lipatov, *Sov. J. Nucl.* **15**, 438 (1972).
54. G. Altarelli and G. Parisi, *Nucl. Phys.* **B126**, 298 (1977).
55. Y. Dokshitzer, *Sov. J. Nucl.* **46**, 641 (1977).
56. ATLAS Collaboration (2012), ATLAS-CONF-2012-100.
57. E. L. Berger, C. Jackson, S. Quackenbush and G. Shaughnessy, *Phys.Rev.* **D84**, 074021 (2011), [arXiv:1107.3150 \[hep-ph\]](#).
58. ATLAS Collaboration, G. Aad *et al.*, *New J.Phys.* **15**, 033038 (2013), [arXiv:1301.6872 \[hep-ex\]](#).
59. . Kramer, Michael, F. I. Olness and D. E. Soper, *Phys.Rev.* **D62**, 096007 (2000), [arXiv:hep-ph/0003035 \[hep-ph\]](#).
60. J. C. Collins, *Phys.Rev.* **D58**, 094002 (1998), [arXiv:hep-ph/9806259 \[hep-ph\]](#).
61. M. Aivazis, J. C. Collins, F. I. Olness and W.-K. Tung, *Phys.Rev.* **D50**, 3102 (1994), [arXiv:hep-ph/9312319 \[hep-ph\]](#).
62. J. Pumplin, D. Stump, J. Huston, H. Lai, P. M. Nadolsky *et al.*, *JHEP* **0207**, 012 (2002), [arXiv:hep-ph/0201195 \[hep-ph\]](#).
63. R. Thorne and R. Roberts, *Phys.Rev.* **D57**, 6871 (1998), [arXiv:hep-ph/9709442 \[hep-ph\]](#).
64. R. Thorne, *Phys.Rev.* **D73**, 054019 (2006), [arXiv:hep-ph/0601245 \[hep-ph\]](#).
65. A. Martin, W. Stirling, R. Thorne and G. Watt, *Eur.Phys.J.* **C70**, 51 (2010), [arXiv:1007.2624 \[hep-ph\]](#).
66. M. Cacciari, M. Greco and P. Nason, *JHEP* **9805**, 007 (1998), [arXiv:hep-ph/9803400 \[hep-ph\]](#).
67. R. D. Ball, V. Bertone, F. Cerutti, L. Del Debbio, S. Forte *et al.*, *Nucl.Phys.* **B849**, 296 (2011), [arXiv:1101.1300 \[hep-ph\]](#).
68. L. Bourhis, M. Fontannaz and J. P. Guillet, *Eur. Phys. J.* **C2**, 529 (1998), [arXiv:hep-ph/9704447](#).
69. A. Gehrmann-De Ridder and E. N. Glover, *Eur.Phys.J.* **C7**, 29 (1999), [arXiv:hep-ph/9806316 \[hep-ph\]](#).
70. S. Frixione, *Phys.Lett.* **B429**, 369 (1998), [arXiv:hep-ph/9801442 \[hep-ph\]](#).

34 *Febres Cordero, and Reina*

71. Z. Bern, G. Diana, L. Dixon, F. Febres Cordero, S. Hoche *et al.*, *Phys.Rev.* **D84**, 114002 (2011), [arXiv:1106.1423 \[hep-ph\]](#).
72. Z. Bern, G. Diana, L. Dixon, F. Febres Cordero, S. Hche *et al.*, *Phys.Rev.* **D87**, 034026 (2013), [arXiv:1206.6064 \[hep-ph\]](#).
73. D0 Collaboration, V. Abazov *et al.*, *Phys.Rev.Lett.* **94**, 161801 (2005), [arXiv:hep-ex/0410078 \[hep-ex\]](#).
74. CMS Collaboration, S. Chatrchyan *et al.*, *JINST* **8**, P04013 (2013), [arXiv:1211.4462 \[hep-ex\]](#).
75. I. W. Stewart and F. J. Tackmann, *Phys.Rev.* **D85**, 034011 (2012), [arXiv:1107.2117 \[hep-ph\]](#).
76. A. Martin, W. Stirling, R. Thorne and G. Watt, *Eur.Phys.J.* **C63**, 189 (2009), [arXiv:0901.0002 \[hep-ph\]](#).
77. H.-L. Lai, M. Guzzi, J. Huston, Z. Li, P. M. Nadolsky *et al.*, *Phys.Rev.* **D82**, 074024 (2010), [arXiv:1007.2241 \[hep-ph\]](#).
78. R. D. Ball, V. Bertone, S. Carrazza, C. S. Deans, L. Del Debbio *et al.*, *Nucl.Phys.* **B867**, 244 (2013), [arXiv:1207.1303 \[hep-ph\]](#).
79. S. Hoeche, F. Krauss and M. Schonherr, *Phys.Rev.* **D90**, 014012 (2014), [arXiv:1401.7971 \[hep-ph\]](#).
80. A. Lipatov and N. Zotov, *J.Phys.* **G34**, 219 (2007), [arXiv:hep-ph/0507243 \[hep-ph\]](#).
81. A. Lipatov, M. Malyshev and N. Zotov, *JHEP* **1205**, 104 (2012), [arXiv:1204.3828 \[hep-ph\]](#).